

Carbon in Si_{1-x}Ge_x Heterojunction Bipolar Transistors

Louis DeWolf Lanzerotti

A DISSERTATION
PRESENTED TO THE FACULTY
OF PRINCETON UNIVERSITY
IN CANDIDACY FOR THE DEGREE
OF DOCTOR OF PHILOSOPHY

RECOMMENDED FOR ACCEPTANCE
BY THE DEPARTMENT OF
ELECTRICAL ENGINEERING

NOVEMBER 1998

This work was supported by
ONR (N00014-96-1-0334),
AFOSR (AASERT F49620-95-1-0438), and
Princeton Program in Plasma Science and Technology (DOE DE-AC 02-76-CH0-3073)

**Carbon in Si_{1-x}Ge_x Heterojunction Bipolar
Transistors**

Louis DeWolf Lanzerotti

**A DISSERTATION
PRESENTED TO THE FACULTY
OF PRINCETON UNIVERSITY
IN CANDIDACY FOR THE DEGREE
OF DOCTOR OF PHILOSOPHY**

**RECOMMENDED FOR ACCEPTANCE
BY THE DEPARTMENT OF
ELECTRICAL ENGINEERING**

NOVEMBER 1998

"When you publish, you are contributing something to society. That is an important responsibility. Before you publish you must try to prove yourself wrong."

Sam McCall 1940-1995

"In the early stages of any development its pursuers do a certain amount of groping in the dark. Techniques are stumbled upon for which the only justification is that they seem to work, even though at the time there is no apparent logical basis. Such processes and items of experience, resembling witchcraft and folklore, are frequently very valuable but should always be handled critically. Transistor processing in the initial stages of its development included a considerable amount of this kind of element."

L. W. Hussey and J. N. Shive 1958

© Copyright 1997 by Louis DeWolf Lanzerotti.
All rights reserved.

Abstract

We have used rapid thermal chemical vapor deposition along with a zero thermal budget transistor process to demonstrate the first Si/Si_{1-x-y}Ge_xC_y/Si heterojunction bipolar transistors (HBT) and to investigate the influence of carbon incorporation on the electrical characteristics of Si_{1-x}Ge_x HBTs. We have used the temperature dependence of transistor collector saturation currents to measure a difference in bandgap between Si_{1-x-y}Ge_xC_y and Si_{1-x}Ge_x of +26 meV/%C for carbon fractions less than 1%.

We have used Si_{1-x-y}Ge_xC_y base HBTs to discover that high carbon concentrations have a profound influence on boron diffusion in Si_{1-x-y}Ge_xC_y alloys. Using the electrical characteristics of these transistors, we demonstrate that thermal diffusion of boron is reduced in Si_{1-x-y}Ge_xC_y alloys. As measured both electrically and by SIMS, boron transient enhanced diffusion caused by an arsenic emitter implant and activation anneal is suppressed in Si_{1-x-y}Ge_xC_y alloys. However, we show that for these discoveries to be useful in HBT applications, the doped Si_{1-x-y}Ge_xC_y base layers must be separated from the transistor depletion regions by doped, carbon-free Si_{1-x}Ge_x spacer layers. These results are explained qualitatively. This discovery of the positive effects of carbon incorporation on boron diffusion may enable Si_{1-x}Ge_x HBTs to be more easily integrated with mainstream silicon technology.

Acknowledgments

Much thanks go to Sam McCall and Bernie Yurke who introduced me to good research techniques at ATT Bell Laboratories the summer before I started at Princeton. Although I haven't always lived up to Sam's admonishments, I think he would be relatively happy with this thesis.

George Kaminsky deserves the most credit for enabling me to eventually get my high frequency, super-self-aligned transistor process working. I would have never been able to make ~ 25 GHz f_T , f_{\max} SiGe HBTs without his valuable contributions.

I owe Venki more than words can describe for taking me under his wing during the late Summer and Fall of 1993. He started me off on the right foot in terms of lithography, wet etching, plasma etching, plasma deposition, probing, oxidation, mask manipulation, leak checking, evaporation, and, most importantly of all, attitude, all while trying to write his own thesis. His help will not be forgotten.

Many thanks go to Anthony St. Amour for teaching me how to grow. The wafers used to obtain the results of this thesis were obtained as much through his efforts as well as through mine. His patience leak checking and fighting with DCS and hydrogen purifiers led directly to the results of this thesis. His efforts never went unappreciated.

Chialin didn't mind me leaning on him during two extended periods of time during my Ph.D. experience. Although we disagreed regularly about the condition of the reactor, this thesis could never have been completed without his help.

A number of "giants" taught me a lot, including Kurdak, Lloyd Engel, Sanjay Parihar, Mike Lange, and Mike Valenti. It is unfortunate that new students will not have the chance to know all of these characters.

And of course there are my peers, (sometime) friends, and associates who made life interesting during the last five years, which, looking back now, seem to have passed rather quickly. Among them are Grayson, Pierre Mertz, Hari, Sanjeev, Luman, Yutaka, Taylor, Wei-pan, George Williams, and Venkat.

Among professors, I would like to especially thank Steve Lyon and Prof. Tsui. Betty Steward was greatly missed during the last half of my years in Princeton.

Outside of Electrical Engineering, thanks goes to Dan Quiram and Chiajen Lay of Chemical Engineering who provided terrific X-Ray service, Temel of Evans East for all the SIMS work, and Eric Stach of University of Virginia who provided all the TEM data used in this thesis.

Thanks also goes to Prof. J. C. Sturm, in whose laboratory this work was performed, for allowing the completion of this dissertation and to Prof. Lyon and Prof. Kahn for taking the time to read this manuscript.

Lastly, I would like to thank Karen Williams for all her help in finishing up this dissertation.

Contents

| | |
|---|-----|
| Abstract | iii |
| Acknowledgments | iv |
| 1 Introduction | 1 |
| 1.1 Motivation | 1 |
| 1.2 Thesis Outline | 2 |
| 2 SiGe and SiGe HBTs | 4 |
| 2.1 An Introduction to Strained $\text{Si}_{1-x}\text{Ge}_x$ on Si Substrates | 4 |
| 2.2 Bandgap of Strained $\text{Si}_{1-x}\text{Ge}_x$ | 8 |
| 2.3 $\text{Si}_{1-x}\text{Ge}_x$ in Bipolar Transistors | 11 |
| 2.4 Bipolar Transistor Theory | 16 |
| 2.5 Summary | 18 |
| 3 Growth and Processing of $\text{Si}_{1-x}\text{Ge}_x$ HBTs | 20 |
| 3.1 Introduction to the Growth of $\text{Si}_{1-x}\text{Ge}_x$ HBTs at Princeton | 20 |
| 3.2 The $\text{Si}_{1-x}\text{Ge}_x$ HBT Process | 29 |
| 3.3 Summary | 31 |

| | | |
|-------|--|----|
| 4 | Si _{1-x} Ge _x HBTs in the Real World | 32 |
| 4.1 | Introduction | 32 |
| 4.2 | Bipolar Transistor Experiments | 33 |
| 4.3 | Non-Ideal Si _{1-x} Ge _x HBT Base Currents | 36 |
| 4.3.1 | Quasi-Ideal Base Current HBTs with Heavily Doped Emitters | 44 |
| 4.4 | Boron Outdiffusion in SiGe HBTs | 54 |
| 4.4.1 | Outdiffusion Theory | 56 |
| 4.4.2 | Outdiffusion Experiments | 60 |
| 4.5 | A Final Note | 64 |
| 4.6 | Summary | 65 |
| 5 | Introduction to Carbon in Si and Si _{1-x} Ge _x | 66 |
| 5.1 | Motivation for Carbon in Si-based Alloys | 66 |
| 5.2 | Early Work on Carbon in Silicon | 67 |
| 5.3 | RTCVD Growth of Si _{1-x-y} Ge _x C _y Alloys at Princeton | 68 |
| 5.4 | Review of Research on Si-based Carbon Alloys | 73 |
| 5.5 | Strain Compensation by Boron | 77 |
| 5.6 | Summary | 77 |
| 6 | Measurement of Si _{1-x-y} Ge _x C _y Bandgap Using HBTs | 78 |
| 6.1 | Introduction | 78 |
| 6.2 | Transistor Characteristics of Si _{1-x-y} Ge _x C _y HBTs | 79 |
| 6.3 | Effect of Carbon on Si _{1-x} Ge _x Bandgap | 82 |
| 6.4 | Bandgap vs Strain for Si _{1-x-y} Ge _x C _y and Si _{1-x} Ge _x | 87 |

| | | |
|----------|--|------------|
| 6.5 | Base Currents in $\text{Si}_{1-x-y}\text{Ge}_x\text{C}_y$ HBTs | 90 |
| 6.6 | Summary | 94 |
| 7 | The Effects of Carbon on Boron Diffusion in SiGe HBTs | 96 |
| 7.1 | Introduction | 96 |
| 7.2 | HBT Process using Emitter and Extrinsic Base Ion Implanted Contacts | 97 |
| 7.3 | Transient Enhanced Diffusion | 99 |
| 7.4 | Introduction to Transient Enhanced Diffusion along with an Historical Perspective on $\text{Si}_{1-x}\text{Ge}_x$ HBTs | 100 |
| 7.5 | Effect of Extrinsic Base Implants on Boron TED in $\text{Si}/\text{Si}_{1-x-y}\text{Ge}_x\text{C}_y/\text{Si}$ HBTs | 103 |
| 7.6 | Effect of Carbon on Thermal Diffusion of Boron . . | 109 |
| 7.7 | Effect of Carbon on Transient Enhanced Diffusion caused by an Arsenic Emitter Implant and Anneal | 115 |
| 7.8 | Problems in HBTs Caused by Carbon | 119 |
| 7.9 | Sandwich Base $\text{Si}_{1-x-y}\text{Ge}_x\text{C}_y$ HBTs | 125 |
| 7.10 | Qualitative Explanation of Experimental Data | 129 |
| 7.11 | A Final Note | 135 |
| 7.12 | Summary | 137 |
| 8 | Conclusion | 139 |
| 8.1 | Summary | 139 |
| 8.2 | Future Work | 140 |

| | |
|---|------------|
| References | 143 |
| A Publications and Presentations Resulting from this Thesis | 156 |
| B Growth Sequence of Si_{0.8}Ge_{0.2} Base HBT | 158 |

List of Figures

| | | |
|------|--|----|
| 2.1 | SiGe/Si interfaces | 5 |
| 2.2 | Si _{1-x} Ge _x critical thickness | 7 |
| 2.3 | Bandgap of strained and unstrained Si _{1-x} Ge _x | 9 |
| 2.4 | Band lineup of strained Si _{1-x} Ge _x on a (100) silicon substrate | 10 |
| 2.5 | Band diagram of a Si _{1-x} Ge _x HBT and a Si BJT | 12 |
| 2.6 | Gummel Plot of Si _{0.8} Ge _{0.2} HBT and a Si BJT | 14 |
| 3.1 | The Princeton rapid thermal CVD reactor | 21 |
| 3.2 | Germanium profiles of six wafers with three different thicknesses | 23 |
| 3.3 | Growth sequence for a typical Si _{0.8} Ge _{0.2} HBT | 26 |
| 3.4 | SIMS of a typical Si _{0.8} Ge _{0.2} HBT doped 10 ²⁰ cm ⁻³ with boron | 27 |
| 3.5 | Growth rate nonuniformity in Princeton RTP chamber | 28 |
| 3.6 | Process for fabricating double mesa SiGe HBTs | 30 |
| 4.1 | Collector Currents for Si _{0.8} Ge _{0.2} HBTs with doped base thicknesses of 50, 100, 200 Å | 34 |
| 4.2 | SIMS of Si _{0.8} Ge _{0.2} Base HBTs with Si _{0.8} Ge _{0.2} thicknesses of 150, 200, and 300 Å | 35 |
| 4.3 | Trap related diode leakage currents | 38 |
| 4.3a | Standard diode recombination currents. | 39 |
| 4.4 | Gummel plot of HBTs grown with Silane and DCS emitters | 40 |
| 4.5 | Detail of base region in a SiGe HBT grown with a Silane emitter | 42 |
| 4.6 | Detail of base region in a SiGe HBT grown with a DCS emitter | 43 |

| | | |
|------|---|----|
| 4.7 | Electrical characteristics of double mesa HBTs with quasi-ideal base currents | 45 |
| 4.8 | Comparison of quasi-ideal base current HBTs with DCS emitter HBTs | 46 |
| 4.9 | SIMS of a SiGe HBT with quasi-ideal base currents | 48 |
| 4.10 | Spreading resistance profile of a SiGe HBT with quasi-ideal base currents | 49 |
| 4.11 | SIMS detail of the base region in an HBT with quasi-ideal base currents | 50 |
| 4.12 | System pressure and oxygen concentration during the growth of the lightly doped emitter | 51 |
| 4.13 | Electrical comparison of HBT with spacers and an outdiffused HBT | 55 |
| 4.14 | Band structure of an outdiffused SiGe HBT | 57 |
| 4.15 | Band structure of a SiGe HBT with a conduction band barrier at the base-collector junction | 58 |
| 4.16 | Transistor characteristics of SiGe HBTs with different spacer widths | 61 |
| 4.17 | Common emitter characteristics for SiGe HBTs from different parts of a wafer | 63 |
| 5.1 | X-ray spectra of $\text{Si}_{1-x-y}\text{Ge}_x\text{C}_y$ wafers with varying carbon fractions | 69 |
| 5.2 | SIMS comparison of a $\text{Si}_{0.8}\text{Ge}_{0.2}$ base with a $\text{Si}_{0.795}\text{Ge}_{0.2}\text{C}_{0.005}$ base | 71 |
| 5.3 | Carbon fraction vs methylsilane flow | 72 |
| 5.4 | X-ray spectra of $\text{Si}_{0.731}\text{Ge}_{0.25}\text{C}_{0.019}$ sample | 74 |
| 5.5 | Cross section TEM micrograph of $\text{Si}_{0.731}\text{Ge}_{0.25}\text{C}_{0.019}$ sample | 75 |

| | | |
|------|---|-----|
| 6.1 | Electrical characteristics of $\text{Si}_{0.8}\text{Ge}_{0.2}$ and $\text{Si}_{0.795}\text{Ge}_{0.2}\text{C}_{0.005}$ base HBTs | 80 |
| 6.2 | Gummel plot of HBTs with three different base carbon concentrations | 81 |
| 6.3 | $\text{Si}_{0.743}\text{Ge}_{0.25}\text{C}_{0.007}$ collector currents as a function of temperature | 84 |
| 6.4 | Normalized collector currents vs inverse temperature | 85 |
| 6.5 | ΔE_G vs carbon fraction | 86 |
| 6.6 | Tradeoffs between bandgap and strain for SiGe and SiGeC alloys | 88 |
| 6.7 | SiGeC sandwich base structure | 91 |
| 6.8 | Common base characteristics of SiGeC sandwich base HBTs | 93 |
| 6.9 | Minority carrier lifetime vs carbon concentration | 95 |
| 7.1 | Ideal-base current HBT process using implantation | 98 |
| 7.2 | SIMS profiles comparing transient enhanced diffusion and thermal diffusion | 101 |
| 7.3 | Transistors fabricated using extrinsic base implantation | 104 |
| 7.4 | Figure 7.3 transistors fabricated using a double mesa process | 106 |
| 7.5 | SIMS measurements showing TED reduction in carbon doped boron superlattices | 108 |
| 7.6 | $\text{Si}_{0.8}\text{Ge}_{0.2}$ and $\text{Si}_{0.795}\text{Ge}_{0.2}\text{C}_{0.005}$ collector currents fabricated from pieces annealed at various temperatures | 110 |
| 7.6b | $\text{Si}_{0.8}\text{Ge}_{0.2}$ and $\text{Si}_{0.795}\text{Ge}_{0.2}\text{C}_{0.005}$ base currents fabricated from pieces annealed at various temperatures | 111 |
| 7.7 | Common emitter characteristics of $\text{Si}_{0.8}\text{Ge}_{0.2}$ and $\text{Si}_{0.795}\text{Ge}_{0.2}\text{C}_{0.005}$ base HBTs fabricated from pieces annealed at 855°C for 15 minutes | 112 |

| | | |
|------|--|-----|
| 7.8 | SIMS of $\text{Si}_{0.8}\text{Ge}_{0.2}$ and $\text{Si}_{0.795}\text{Ge}_{0.2}\text{C}_{0.005}$ wafers following 855°C anneal | 114 |
| 7.9 | SIMS of arsenic implant following 755°C, 15 minute anneal | 116 |
| 7.10 | Device cross section for devices fabricated using an arsenic implanted emitter | 117 |
| 7.11 | $\text{Si}_{0.8}\text{Ge}_{0.2}$ and $\text{Si}_{0.795}\text{Ge}_{0.2}\text{C}_{0.005}$ device characteristics from wafer pieces following arsenic implantation and 647°C, 15 minute anneal | 118 |
| 7.12 | SIMS of $\text{Si}_{0.8}\text{Ge}_{0.2}$ and $\text{Si}_{0.795}\text{Ge}_{0.2}\text{C}_{0.002}$ wafers following arsenic implantation and 755°C, 15 minute anneal | 120 |
| 7.13 | $\text{Si}_{0.8}\text{Ge}_{0.2}$ and $\text{Si}_{0.795}\text{Ge}_{0.2}\text{C}_{0.005}$ device characteristics from wafer pieces following arsenic implantation and 750°C anneal | 121 |
| 7.14 | $\text{Si}_{0.8}\text{Ge}_{0.2}$ and $\text{Si}_{0.795}\text{Ge}_{0.2}\text{C}_{0.005}$ base-emitter I-V curves for as-grown devices and for devices following arsenic implantation and 750°C anneal | 123 |
| 7.15 | $\text{Si}_{0.8}\text{Ge}_{0.2}$ and $\text{Si}_{0.795}\text{Ge}_{0.2}\text{C}_{0.005}$ base-collector I-V curves for as-grown devices and for devices following arsenic implantation and 750°C anneal | 124 |
| 7.16 | $\text{Si}_{0.795}\text{Ge}_{0.2}\text{C}_{0.005}$ sandwich base transistor characteristics from wafer pieces following arsenic implantation and 742°C anneal | 126 |
| 7.17 | SIMS from as-grown sandwich base wafers as well as for sandwich base wafer following arsenic implantation and 755°C, 15 minute anneal | 128 |
| 7.18 | Interstitial concentration during activation anneal following arsenic emitter implant for SiGe and SiGeC HBTs | 130 |

| | | |
|------|--|-----|
| 7.19 | Interstitial concentration during activation anneal following arsenic emitter implant for SiGeC sandwich base HBTs | 132 |
| 7.20 | Comic illustrating the possible mechanism through which carbon atoms trap silicon interstitial atoms | 134 |
| 7.21 | TEM micrographs comparing SiGe and SiGeC bases following arsenic emitter implantation and high temperature annealing | 136 |

Chapter 1

Introduction

1.1 Motivation

Although virtually every review article on $\text{Si}_{1-x}\text{Ge}_x$ alloys includes a statement to the effect that $\text{Si}_{1-x}\text{Ge}_x$ "electronic devices ... can be fabricated on silicon substrates with only minor deviations from well-established silicon integrated circuit technology" [1], as of mid-1997, an integrated circuit which includes $\text{Si}_{1-x}\text{Ge}_x$ alloys is not commercially available. This thesis addresses two fundamental factors which currently limit $\text{Si}_{1-x}\text{Ge}_x$ technology. The first problem pertains to limits on $\text{Si}_{1-x}\text{Ge}_x$ alloy thickness. The second problem pertains to boron diffusion in $\text{Si}_{1-x}\text{Ge}_x$ alloys. This thesis uses the bipolar transistor device structure as a test vehicle to try to solve these problems.

A heterojunction, that is a material of a certain bandgap on top of a material of another bandgap, can lead to improved device performance if the heterojunction is strategically well placed within the device [2-4]. This work focuses on two heterojunctions, the $\text{Si}/\text{Si}_{1-x}\text{Ge}_x$ heterojunction and the $\text{Si}/\text{Si}_{1-x-y}\text{Ge}_x\text{C}_y$ heterojunction,

in the context of the bipolar transistor device. While the fundamental physical advantages and limitations of the SiGe/Si heterojunction were well mapped out prior to the beginning of this work in 1993 [5-7], the effect of carbon incorporation in $\text{Si}_{1-x}\text{Ge}_x$ on the Si/ $\text{Si}_{1-x}\text{Ge}_x$ heterojunction is newly explored using bipolar transistors in this thesis.

A $\text{Si}_{0.8}\text{Ge}_{0.2}$ thin film above 100 Å in thickness is prone to defect formation. By adding small amounts of substitutional carbon to a $\text{Si}_{1-x}\text{Ge}_x$ layer, creating the new ternary alloy $\text{Si}_{1-x-y}\text{Ge}_x\text{C}_y$, one may relax this limit on alloy thickness. This thesis uses $\text{Si}_{1-x-y}\text{Ge}_x\text{C}_y$ base heterojunction bipolar transistors to measure the effects of carbon on electrical properties and to measure the effects of carbon incorporation on the $\text{Si}_{1-x}\text{Ge}_x$ bandgap.

Although 10^{20} cm^{-3} base boron concentrations are desirable for high frequency transistor operation, manufacturable $\text{Si}_{1-x}\text{Ge}_x$ base heterojunction bipolar transistor processes currently limit boron concentrations to $\sim 3 \times 10^{18} \text{ cm}^{-3}$ [8,9]. The diffusion of boron during process integration prevents the use of higher dopant concentrations. The research presented in this thesis discovered that carbon has the ability to reduce boron diffusion in $\text{Si}_{1-x-y}\text{Ge}_x\text{C}_y$ alloys. Using these results, superior transistors have been demonstrated which would have been impossible to fabricate without the addition of carbon to the $\text{Si}_{1-x}\text{Ge}_x$ base.

1.2 Thesis Outline

Chapter 2 introduces strained $\text{Si}_{1-x}\text{Ge}_x$ alloys and HBT theory and experiments. The chapter contains background material useful for the entire thesis.

$$V_A = \frac{qn_i^2(W_B)D_n(W_B)}{C_{BC}} \left(\int_0^{W_B} \frac{N_A dx}{n_i^2 D_n} \right) \quad [2.5]$$

where $n_i(W_B)$ and $D_n(W_B)$ are the intrinsic carrier concentration and minority carrier diffusion coefficients, respectively, evaluated at the collector edge of the base. C_{BC} is the base-collector capacitance.

In the case of a SiGe HBT with constant germanium fraction and doping in the base, Equation 2.5 reduces to

$$V_A = \frac{qN_A W_B}{C_{BC}} \quad [2.6]$$

Since C_{BC} is determined by the width of the lightly doped collector, higher base dopings lead directly to higher Early voltages.

2.5 Summary

This chapter has served as an introduction to the SiGe material system and SiGe heterojunction bipolar transistors. The limitations on SiGe thickness due to strain has been established. The bandgap difference between silicon and strained SiGe is roughly twice that between silicon and unstrained SiGe. The bandgap difference between unstrained silicon and strained SiGe is accommodated almost totally as a valence band offset.

Chapter 2

SiGe and SiGe HBTs

2.1 An Introduction to Strained $\text{Si}_{1-x}\text{Ge}_x$ on Si substrates

$\text{Si}_{1-x}\text{Ge}_x$ is an alloy of germanium atoms mixed in randomly with silicon atoms, as shown in Figure 2.1a. x is that fraction of atoms which are germanium, $1-x$ is that fraction of atoms which are silicon. A $\text{Si}_{1-x}\text{Ge}_x/\text{Si}$ heterojunction may be created by the growth of the alloy $\text{Si}_{1-x}\text{Ge}_x$ on a silicon substrate. For modern electronics, the SiGe layer is grown epitaxially on the industry standard Si (100) substrate although in the past, free standing SiGe crystals have been investigated [10]. Because germanium falls below silicon in column four of the periodic table, it has a larger lattice constant than silicon (4.2%). Thus, a free-standing SiGe thin film not attached to a silicon substrate will have a lattice constant larger than that of pure silicon, as shown in Figures 2.1a and 2.1b.

One may "fit" this larger lattice constant SiGe material on the smaller Si substrate lattice by accommodating the difference in lattice constant through the introduction of misfit dislocations, as shown in Figure 2.1c. This SiGe film is called a relaxed layer because its lattice constant is near that of a free standing film. For minority carrier device

Figure 2.1a: Unstrained SiGe

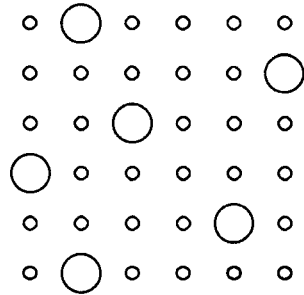


Figure 2.1b: Unstrained Si

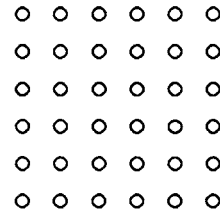
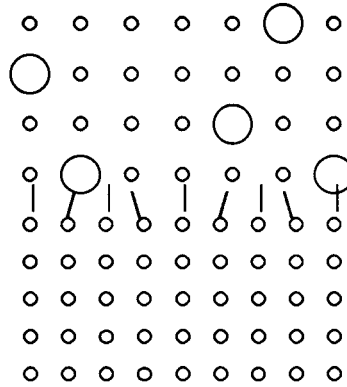


Figure 2.1c: Relaxed SiGe



Silicon Atom:



Germanium Atom:



Figure 2.1d: Strained SiGe

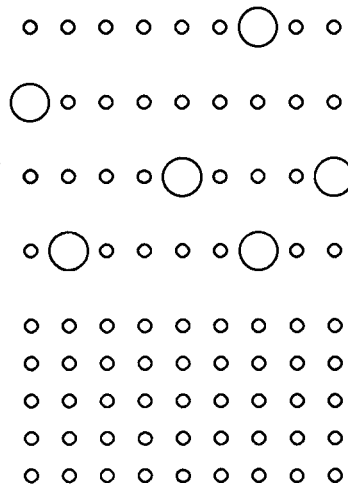


Figure 2.1: SiGe/Si Interfaces.

applications, such as the bipolar transistors to be discussed in this thesis, these dislocations are not desirable since they are recombination sites which decrease current gain by increasing base current [11, 12].

One may also grow a layer of SiGe on silicon by compressing the horizontal lattice constant of the SiGe layer to fit on the substrate Si lattice sites without the introduction of misfit dislocations. This compression of the horizontal SiGe lattice constant leads to an increase in the vertical lattice constant, as shown in Figure 2.1d. The original silicon substrate lattice constant is assumed to be unchanged because the compressed SiGe film on top of the silicon substrate is extremely thin compared with the Si substrate below it. The growth of a dislocation-free SiGe layer on a silicon substrate is called a strained or "pseudomorphic" SiGe film because the SiGe would rather relax to its free standing lattice constant as shown in Figure 2.1a. However, an energy barrier to the formation of dislocations exists which prevents the strained layer from relaxing [13]. Increasing the Ge fraction in a given layer increases the strain in the layer because the difference between unstrained SiGe lattice constant and the silicon substrate increases.

The initial growth of SiGe thin films is in the strained state, and this growth proceeds up to a certain "critical thickness," above which strain is relieved by the incorporation of misfit dislocations. In other words, after a finite critical thickness the SiGe will tend to relax to its unstrained horizontal lattice constant through the introduction of misfit dislocations at the SiGe/Si interface [14].

This critical thickness is plotted as a function of germanium in Figure 2.2 and is the thickness for which the SiGe layer is stable regardless of the heat treatment the layer undergoes. One can grow thicker strained layers than this equilibrium critical thickness; however, exposure to high temperatures will encourage dislocation formation in the SiGe film [7]. Strained films grown above the critical thickness are called metastable films

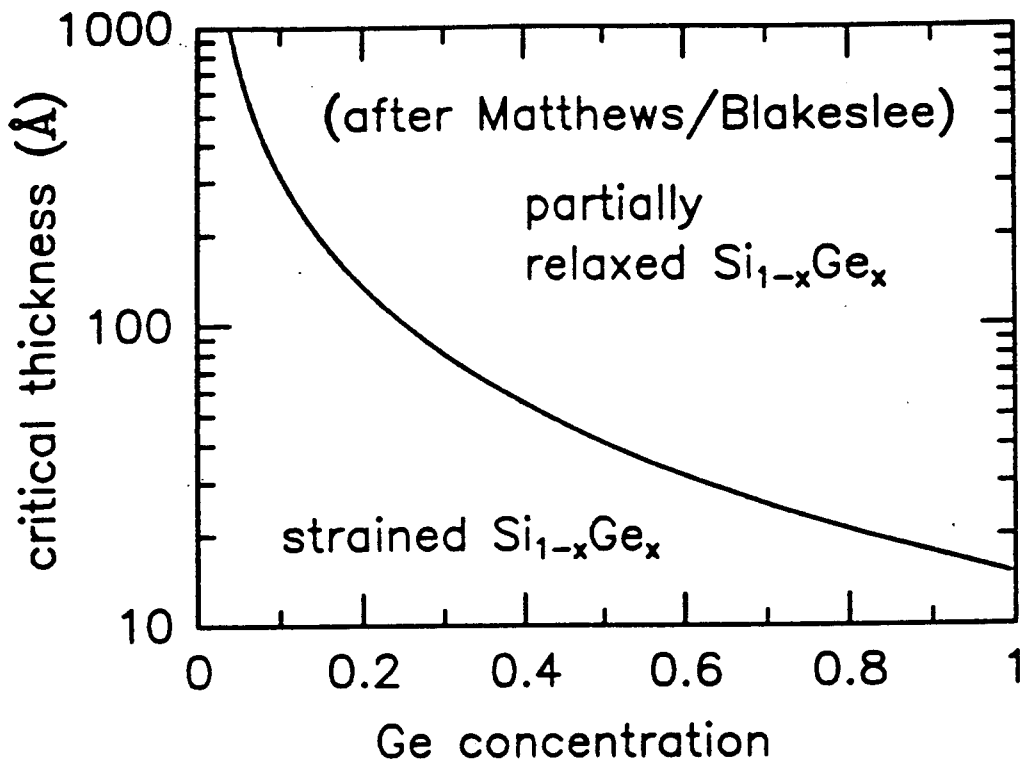


Figure 2.2: Equilibrium critical thickness of strained $\text{Si}_{1-x}\text{Ge}_x$ films on (100) silicon substrates as a function of Ge fraction.

because they will relax to the unstrained lattice constant following high temperature heat treatment. This limitation on SiGe thickness is a fundamental constraint which device engineers are faced with when designing devices which include SiGe heterojunctions.

2.2 Bandgap of Strained $\text{Si}_{1-x}\text{Ge}_x$

The advantage of the SiGe heterojunction stems from the fact that germanium has a smaller bandgap than that of silicon. One may expect then, that as germanium is added to silicon, the bandgap of relaxed SiGe should decrease until the bandgap equals that of germanium at $x=1$. This is indeed the case, as shown in Figure 2.3, which plots relaxed SiGe bandgap as a function of Ge content. The kink at $x=0.8$ is due to the transition from "Si-like" bandstructure to that of "Ge-like" band structure. The bandgap of pseudomorphically strained SiGe on Si (100) substrates is, however, drastically different from that of unstrained SiGe due to the effects of strain on the band structure, as shown in Figure 2.3. As seen in Figure 2.3, the bandgap difference between strained SiGe and Si is roughly double that between unstrained SiGe and Si. The bandgap of strained SiGe is roughly 7 meV/% Ge smaller than that of silicon. In strained SiGe, for all practical purposes, the entire bandgap difference is incorporated in the valence band offset and consequently the conduction band discontinuity is negligible, as shown in Figure 2.4 for an undoped Si/SiGe heterostructure.

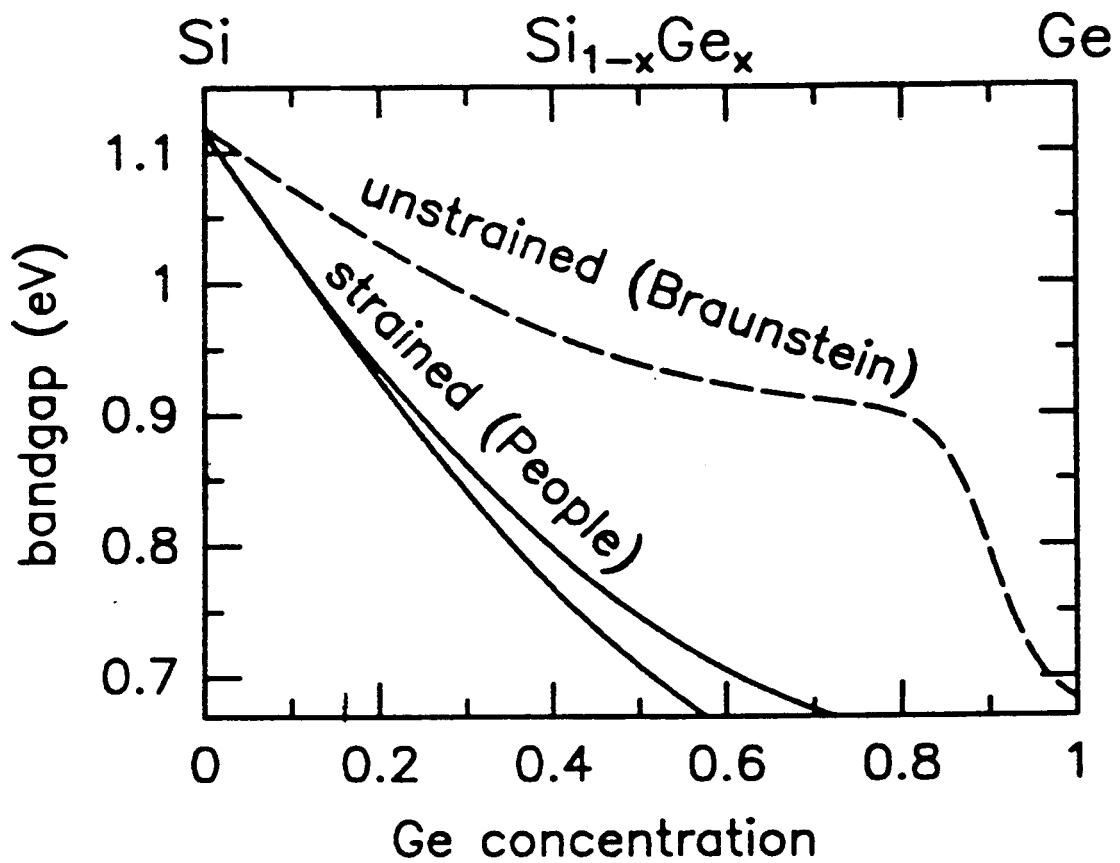


Figure 2.3: Bandgap of unstrained and strained $\text{Si}_{1-x}\text{Ge}_x$ as a function of Ge fraction.

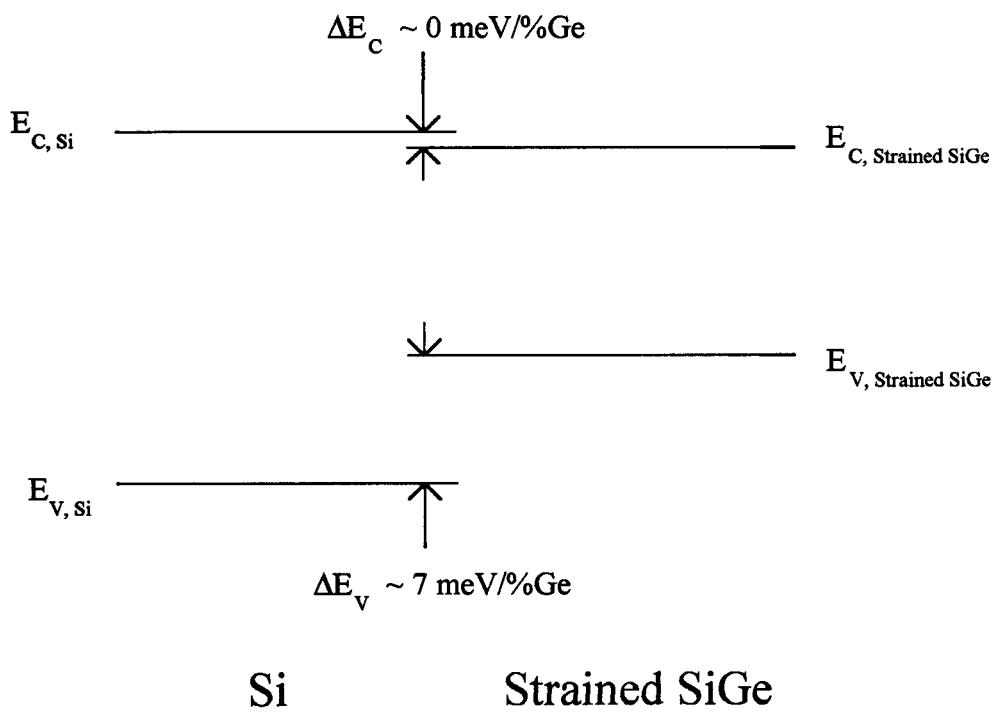


Figure 2.4: Band lineup of strained SiGe alloys on (100) Si Substrates.

2.3 Si_{1-x}Ge_x in Bipolar Transistors

In terms of device applications, strained p-type SiGe can be used effectively as a replacement for the unstrained p-type Si base in a silicon npn bipolar junction transistor (BJT). The incorporation of a SiGe layer in the base of a bipolar transistor creates a new device called a heterojunction bipolar transistor (HBT). However, for SiGe heterojunction bases to be worthwhile for real-world applications, they must lead to performance advantages over that of pure Si bipolar transistors because of the added complications introduced by the epitaxially-grown strained SiGe base.

Figure 2.5 shows the band diagram of an actively biased npn SiGe HBT superimposed on that of an actively biased Si bipolar transistor. This band diagram assumes that base doping is identical in both transistors and no grading of Ge fraction in the base. The distance between the base Fermi level and the valence band in both transistors is the same to first order, because the base doping is identical in both devices (SiGe has a different density of states than that of silicon, however).

Under active biasing of a bipolar transistor, the base-emitter is forward biased while the base collector is reverse biased, as shown in Figure 2.5. This forward-biased emitter-base junction injects electrons into the base, which diffuse across the base, and are then collected by the reverse-biased base collector junction. Since, as shown in Figure 2.5, the barrier for electron injection into the base is lower in strained SiGe than Si due to the smaller SiGe bandgap, more electrons are injected into the SiGe base than the Si base at fixed forward V_{BE} . The lower barrier leads to a higher SiGe collector current than Si collector current at fixed V_{BE} or identically an increased collector saturation current, the collector current (I_C) extrapolated to $V_{BE} = 0$. Since, at fixed V_{BE} , the barrier for hole injection into the Si emitter is constant for both SiGe and Si, the base current (I_B) remains

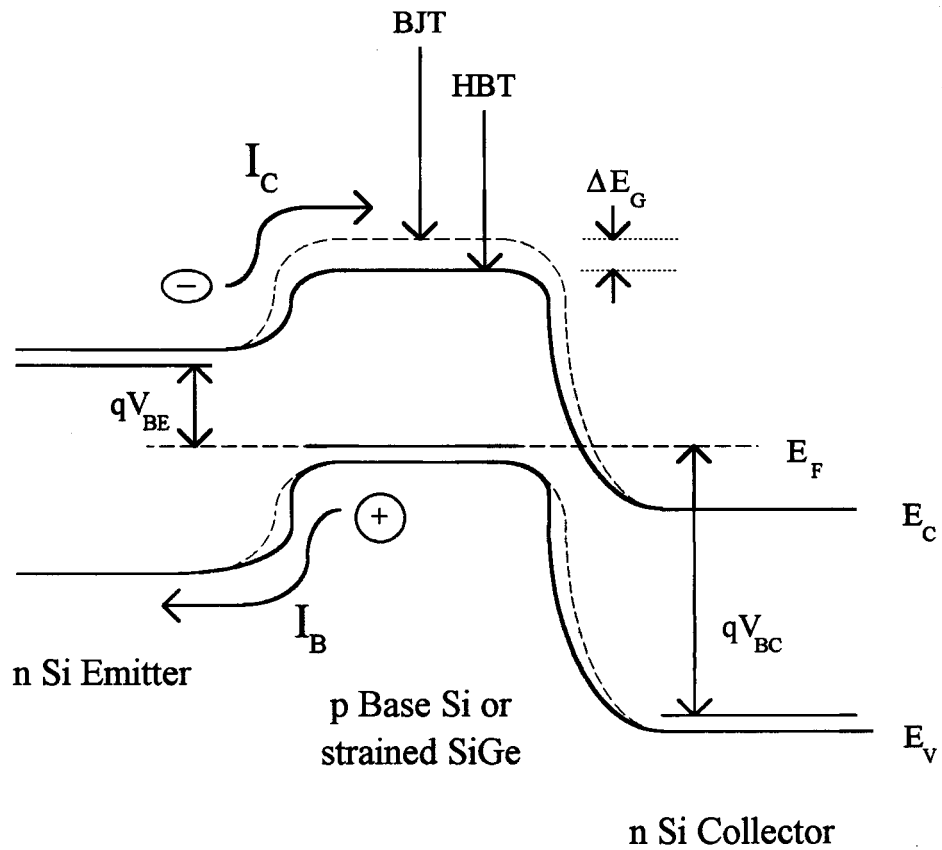


Figure 2.5: The band structure of a n-Si/p-SiGe/n-Si HBT compared to that of a Si BJT.

constant in both devices, assuming that other sources of base current such as recombination in the base are negligible. Since current gain $\beta = I_C/I_B$, the SiGe device has a higher current gain than that of the all Si transistor. The Gummel plot of a $\text{Si}_{0.8}\text{Ge}_{0.2}$ device compared to that of a silicon device, Figure 2.6 [15], shows that the collector current in the SiGe HBT increases relative to that of the Si BJT at fixed V_{BE} , while the base current remains constant. Hence the SiGe HBT has higher β than the Si BJT.

This explanation of the current gain advantages of SiGe HBTs takes the point of view of increasing collector saturation currents with increasing germanium fraction at fixed V_{BE} . One may also look at the current gain advantages of SiGe HBTs from the point of view of fixed collector currents and variable base-emitter voltages. At a fixed collector current, in Figure 2.6, the SiGe base-emitter diode will have a lower V_{BE} than the all Si base-emitter diode. Hence the barrier for hole injection into the emitter will be greater, at fixed collector current, for the SiGe HBT than for the Si BJT. Fewer holes in the HBT emitter will lead to lower base current in the SiGe HBT compared with that of the Si BJT. Thus, from the point of view of fixed collector currents, the current gain in a SiGe device is increased because of the lower base current compared with that of the all Si device. These simple explanations have neglected more complicated effects which have been addressed elsewhere such as dopant induced bandgap narrowing and changes in minority carrier diffusion coefficients and densities of states due to the strained SiGe base [15, 16].

Enormous current gains of the order of 5000 become possible in SiGe base HBTs [5] but are not typically desirable for circuit applications [2]. In other words, the simple current gain advantage of a SiGe HBT over that of a Si BJT is not sufficient to justify using SiGe bases since Si BJT gains are sufficient. However, in SiGe HBTs we may trade this increase in current gain for other device parameters which will allow higher device

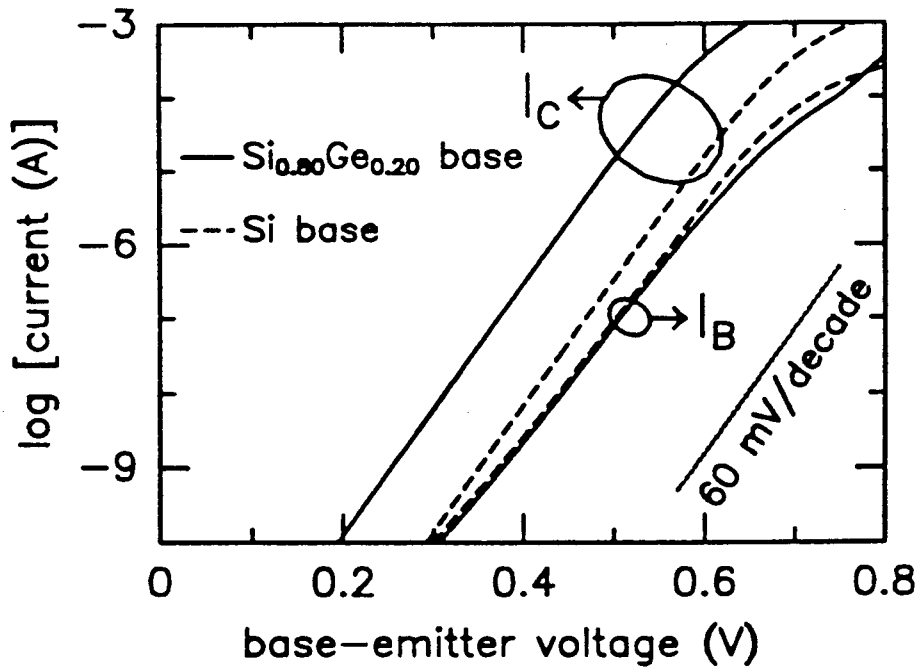


Figure 2.6: Gummel Plot of a $\text{Si}_{0.8}\text{Ge}_{0.2}$ HBT and a Si BJT showing HBT β enhancement due to increase in collector saturation current. [15]

frequency performance than that obtainable with pure silicon bases. For example, by increasing the base doping in the SiGe transistor one can decrease the device's base sheet resistance. Increased base doping leads to a decrease in collector saturation current since collector current is inversely proportional to base doping. Consequently, the current gain of a SiGe transistor with increased base doping is reduced. In a BJT, base doping can not be increased arbitrarily: at the simplest level, the emitter Gummel number (the product of the emitter doping and the width of the emitter) must be greater than the base Gummel number (the product of the base doping and the width of the base) to have $\beta > 1$. However, the smaller bandgap SiGe base, which leads to increased collector currents, enables transistor designers to decouple base doping considerations from current gain in SiGe HBTs. Hence, while additional base doping decreases the current gain by decreasing I_C , heavily doped SiGe base transistors may be designed in which the base doping actually exceeds the emitter doping and yet still have high current gain.

The SiGe HBTs used in this thesis use base doping roughly one order of magnitude greater than the emitter doping. By carefully engineering the germanium content and the width of the base, the devices in this thesis achieved current gains of roughly 50 with base germanium fractions of 20%, base doping concentrations of 10^{20} cm^{-3} , and doped base widths ranging from 50 to 200 Å. This high doping concentration brings about a 1-2 order of magnitude decrease in base sheet resistance compared with typical Si BJTs. Higher SiGe transistor frequency performance compared with that of Si transistors is fundamentally related to this decrease in base sheet resistance. One can also obtain high speed transistors by grading the germanium content across the base. This introduces a built-in field in the base so that electrons move across the base by both drift and diffusion [8].

In addition to increasing frequency performance relative to that of all Si devices, high base doping in SiGe base HBTs can lead to higher Early voltages compared with that of Si BJTs. High transistor Early voltages, a measure of device output resistance at fixed base current, are desirable. A device's Early voltage is a consequence of an increased collector current caused by a widening base-collector space charge region which reduces the transistor base width. Since collector current is inversely related to base width, a decrease in base width caused by an increase in base-collector reverse bias will lead to an increased collector current. If the base is heavily doped, as in the case of SiGe HBTs, the base undergoes much smaller changes in base width for fixed increases in base-collector reverse bias. Smaller changes in base width lead directly to higher Early voltages in heavily doped SiGe HBTs.

2.4 Bipolar Transistor Theory

To fully evaluate the fundamental tradeoffs in SiGe; that of increasing collector current gain with increased germanium fraction, decreased critical thickness with increasing germanium fraction, and increased Early voltage with base doping, one must express this physical understanding in terms of equations.

Assuming that the diffusion length of electrons in the base is much longer than the base width so that neutral base recombination may be neglected, the collector current in a base with constant bandgap and doping is

$$J_C = J_{C_0} e^{qV_{BB}/k_B T} \quad [2.1]$$

The quantity J_{Co} is the collector saturation current density (J_C extrapolated to $V_{BE} = 0$ V) and is a function of $n_{i, base}^2$, the base intrinsic carrier concentration; D_n , the electron diffusion coefficient; N_A , the base doping; and W_B , the base width.

$$J_{Co} = \frac{qD_n n_{i,base}^2}{N_A W_B} \quad [2.2]$$

for constant base doping and Ge concentration. Since

$$n_{i,base}^2 = N_C N_V e^{-E_{G,base}/k_B T} \quad [2.3]$$

a SiGe base with the same doping in the base has an exponentially increased J_{Co} due to the fact that $n_{i,SiGe}^2 \gg n_{i,Si}^2$ since $E_{G, SiGe} < E_{G, Si}$.

For a base which has both a varying bandgap and a varying doping concentration across the base, the generalized equation of collector current under active bias is [17]

$$J_C = q \left(\int_0^{W_B} \frac{\rho(x) dx}{n_i^2(x) D_n(x)} \right)^{-1} e^{qV_{BE}/k_B T} \quad [2.4]$$

While for a base with constant germanium fraction and constant doping level, Equation 2.4 reduces to Equation 2.2, the importance of the generalized collector current expression will become apparent in Chapter 3.

For a transistor with arbitrary base bandgap and doping profiles, the Early voltage is given by [17]

$$V_A = \frac{qn_i^2(W_B)D_n(W_B)}{C_{BC}} \left(\int_0^{W_B} \frac{N_A dx}{n_i^2 D_n} \right) \quad [2.5]$$

where $n_i(W_B)$ and $D_n(W_B)$ are the intrinsic carrier concentration and minority carrier diffusion coefficients, respectively, evaluated at the collector edge of the base. C_{BC} is the base-collector capacitance.

In the case of a SiGe HBT with constant germanium fraction and doping in the base, Equation 2.5 reduces to

$$V_A = \frac{qN_A W_B}{C_{BC}} \quad [2.6]$$

Since C_{BC} is determined by the width of the lightly doped collector, higher base dopings lead directly to higher Early voltages.

2.5 Summary

This chapter has served as an introduction to the SiGe material system and SiGe heterojunction bipolar transistors. The limitations on SiGe thickness due to strain has been established. The bandgap difference between silicon and strained SiGe is roughly twice that between silicon and unstrained SiGe. The bandgap difference between unstrained silicon and strained SiGe is accommodated almost totally as a valence band offset.

Adding germanium to the base of a silicon bipolar transistor increases current gain by increasing collector saturation current. This higher SiGe current gain can be traded for higher base doping concentrations in SiGe HBTs than possible in Si BJTs.

Growth and Processing of $\text{Si}_{1-x}\text{Ge}_x$ HBTs

3.1 Introduction to the Growth of $\text{Si}_{1-x}\text{Ge}_x$ HBTs at Princeton

The wafers used to fabricate the devices used in this thesis were grown by rapid thermal chemical vapor deposition (RTCVD) [18]. The single wafer RTCVD reactor, as shown in Figure 3.1, is a cold-walled system designed to heat and cool wafers more rapidly than possible using conventional hot-walled furnaces. The wafer is introduced into the quartz process chamber through a load lock which is pumped and purged with nitrogen. The wafer is heated from below by a bank of tungsten halogen lamps outside the quartz tube. The wafer and lamps are surrounded by a gold plated reflector assembly. The wafer temperature is actively measured between 550°C and 800°C using changes in wafer transmission of 1.3 and 1.5 mm infrared light [19]. Temperatures of up to 1000°C are possible by calibrating lamp output power with a thermocouple attached to a dummy wafer.

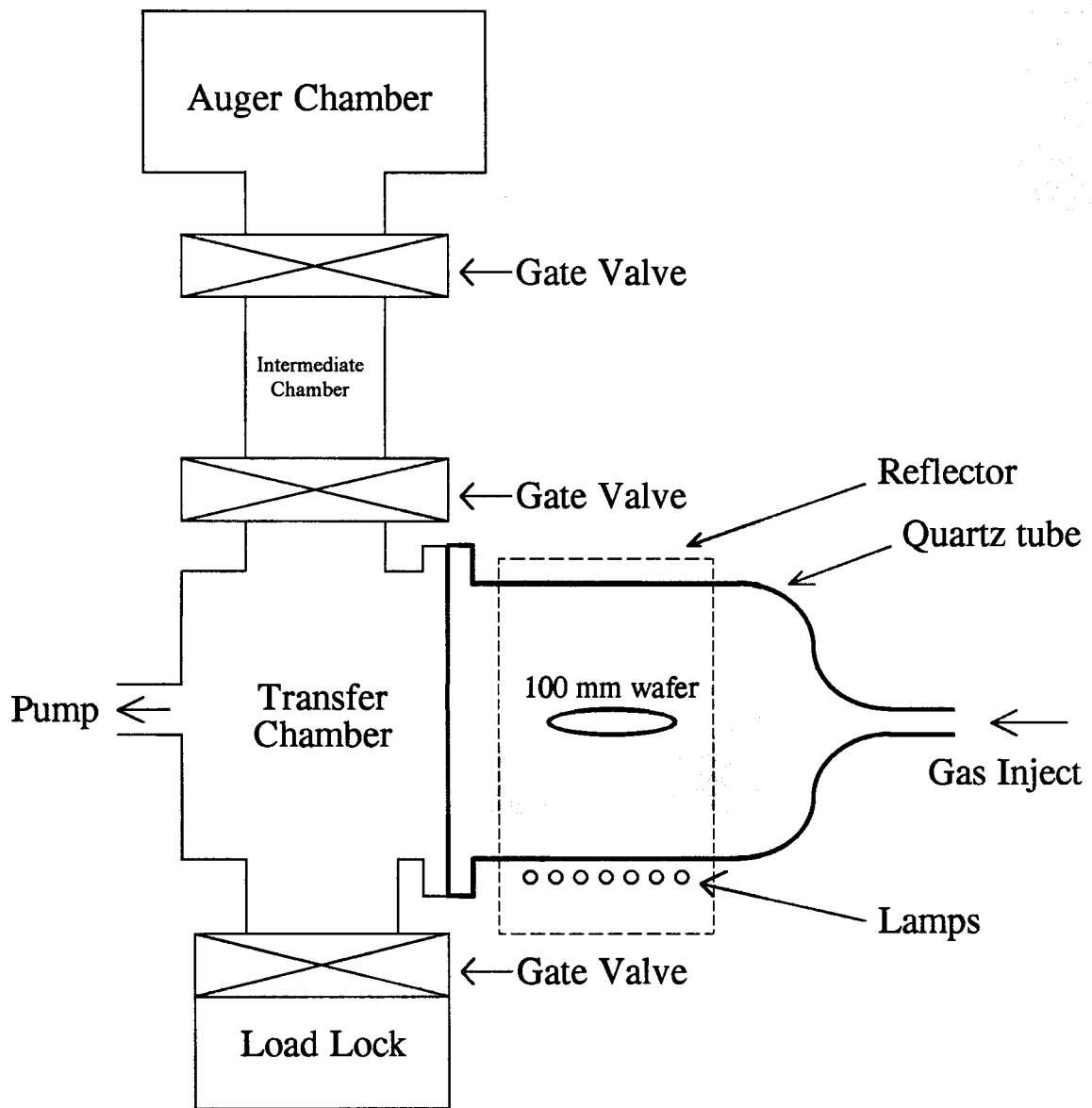


Figure 3.1: The Princeton single wafer rapid thermal CVD reactor.

In this work, double-side polished wafers were used to eliminate the undesirable effects caused by an unpolished backside wafer surface during growth. The room temperature laser transmission of single side polished wafers is limited by backside surface scattering. Hence the room temperature transmission of a double side polished wafer is several orders of magnitude larger than a typical single side polished wafer. The transmission of single side polished wafers also tends to change during growth due to changes in backside surface roughness caused by growth on that surface. This leads to temperature drift during growth and consequently to errors in growth rate caused by a changing baseline transmission value. The author has found that double side polished wafers in this reactor's temperature setup leads to better wafer to wafer thickness control because the baseline room temperature wafer transmission is virtually identical before and after growth. Figure 3.2 shows germanium SIMS profiles of $\text{Si}_{0.8}\text{Ge}_{0.2}$ and $\text{Si}_{0.795}\text{Ge}_{0.2}\text{C}_{0.005}$ wafers with thicknesses of 150, 200, 300 Å from different wafers grown identically except for the inclusion of 0.5% carbon. Note that the Ge profiles are nearly identical between wafers (carbon levels below 1% do not significantly affect SiGe growth rate [20]) showing the excellent run to run reproducibility in this system when double side polished substrates are used. Figure 3.2c shows the as-grown germanium profiles. The germanium profile in Figure 3.2b is that following arsenic emitter implantation and 750°C, 15 minute anneal (Chapter 7). The germanium profile in Figure 3.2a is that following a 850°C, 15 minute anneal (Chapter 7). These two postgrowth processes are not expected to affect the germanium profiles, however.

In addition, since double side polished wafers have far higher room temperature transmission values than single side polished wafers due to the absence of backside laser scattering, temperatures up to 775-810°C may be measured using double side polished wafers in the current setup. With single side polished wafers in this setup, ~775°C is the

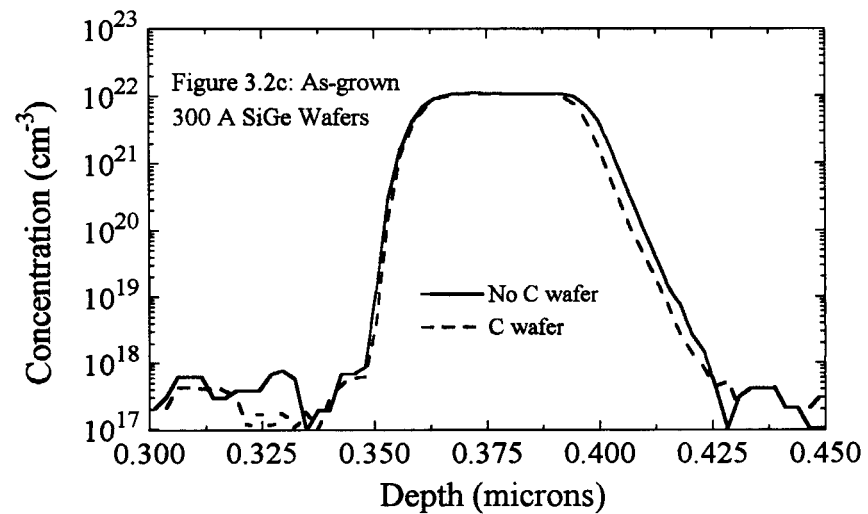
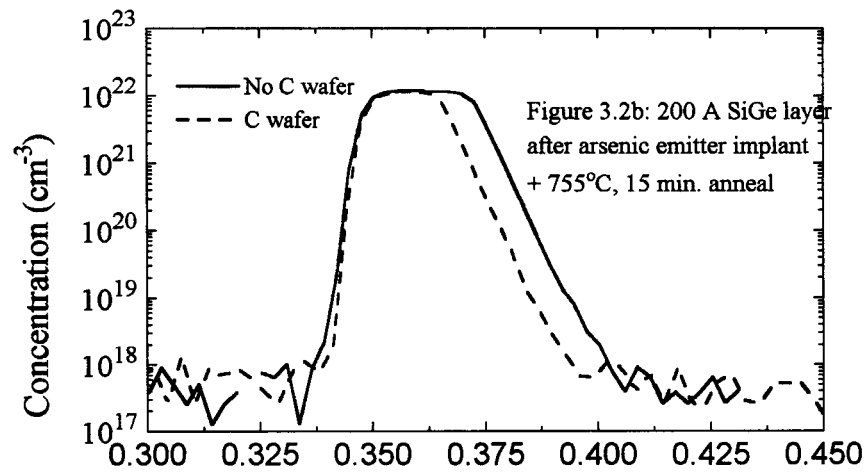
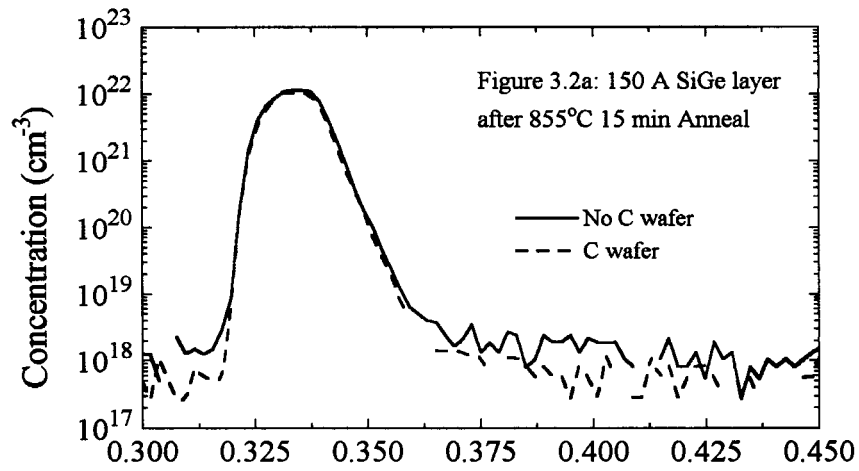


Figure 3.2: SIMS profiles of SiGe and SiGeC bases with three different thicknesses.

maximum measurable temperature because at this temperature, the transmitted signal drops below a minimum detectable level.

The wafers were cleaned using a standard silicon valley clean ($2 \text{ H}_2\text{SO}_4: 1 \text{ H}_2\text{O}_2$) followed by a deionized water rinse. The wafers underwent an HF dip before entering the load lock. The wafer was first heated to 1000°C for one minute at 250 torr with a H_2 flow of 4 slpm to desorb any residual surface SiO_2 . Following the clean, this general transistor structure was grown at 6 torr with a H_2 flow of 3 slpm. First, the subcollector was grown at 1000°C for 5 minutes using 26 sccm dichlorosilane (DCS) and phosphine which resulted in a $2 \times 10^{18} \text{ cm}^{-3}$ μm thick n-type subcollector layer. Following the subcollector, the n-type collector was grown at 1000°C for one minute using DCS without any phosphine flow which resulted in a 2000 \AA mid- 10^{17} cm^{-3} n-type collector doped by residual chamber phosphine from the subcollector growth.

The temperature was then decreased to 625°C to grow the SiGe base layers. Adding germane to DCS results in dramatically increased growth rates compared to pure Si epitaxy [1, 21]. To ensure metastable SiGe thin films as well as controllable growth rates, the wafer temperature is lowered to 625°C to grow SiGe. DCS is kept flowing at all times, even during the temperature ramps. When the wafer temperature has stabilized at 625°C , germane is injected to grow the nominally undoped $\text{Si}_{0.8}\text{Ge}_{0.2}$ spacer layers (lightly doped n-type by residual phosphine) between the Si collector and the p+ SiGe base. The purpose of this spacer layer will be discussed in Chapter 4. The growth rate in this chamber for 20% Ge is $50 \text{ \AA}/\text{min}$ at 625°C for these wafers under these conditions. The thicknesses of the base regions are determined simply by the time during which germane or diborane is injected. Following the undoped spacer layer, the doped $\text{Si}_{0.8}\text{Ge}_{0.2}$ base is grown by injecting diborane. Typical doped base thicknesses used in this thesis ranged from $50 - 200 \text{ \AA}$ with boron concentrations of 10^{20} cm^{-3} .

Following the doped base, another nominally undoped $\text{Si}_{0.8}\text{Ge}_{0.2}$ spacer is grown between the doped base and the doped emitter. Following the SiGe layers, DCS and germane are turned off at same time at which silane is injected. The temperature is then increased to 700°C to grow the emitter layer with silane (100 sccm of 10% SiH_4 in Ar) since the growth rate of silicon at 625°C is too low. PH_3 (25 sccm of 100 ppm PH_3 in H_2) is then injected to grow the 500 \AA $8 \times 10^{18} \text{ cm}^{-3}$ n-type emitter. The PH_3 flow is increased (300 sccm) to grow the 2500 \AA 10^{19} cm^{-3} n-type emitter contact layer. The total emitter growth time is roughly seventy minutes. Silane was used for emitter growth instead of DCS for all wafers discussed in this thesis except those section 4.2. In this reactor, the growth rate of silane at 700°C is comparable to that of the growth rate of DCS at 750°C . Hence, by using silane instead of DCS, the heavily doped, metastable SiGe thin films see a smaller thermal budget during emitter growth. This silane emitter process was developed by Prinz et. al. for growing novel double base SiGe HBTs [22]. A schematic of the different transistor layers is shown in Figure 3.3. Figure 3.4 shows SIMS for a typical transistor used in this thesis.

The epitaxial thicknesses grown in our RTCVD reactor, while azimuthally symmetric, are not uniform from the center of the wafer (where the temperature is measured by infrared transmission) to the edge of the wafer. This is due to the simple reactor design and the fact that the edge of a wafer radiates heat better than does the center. As one moves towards the edge of the 4 inch wafer, the wafer growth temperature is lower, leading to a decreased growth rate. Figure 3.5 plots growth rate as measured by TEM vs. distance from the center of a wafer for two different growth conditions illustrating the large nonuniformities inherent in this system. Note that a growth wafer has a radius of 5 cm. In addition, the temperature difference which leads to

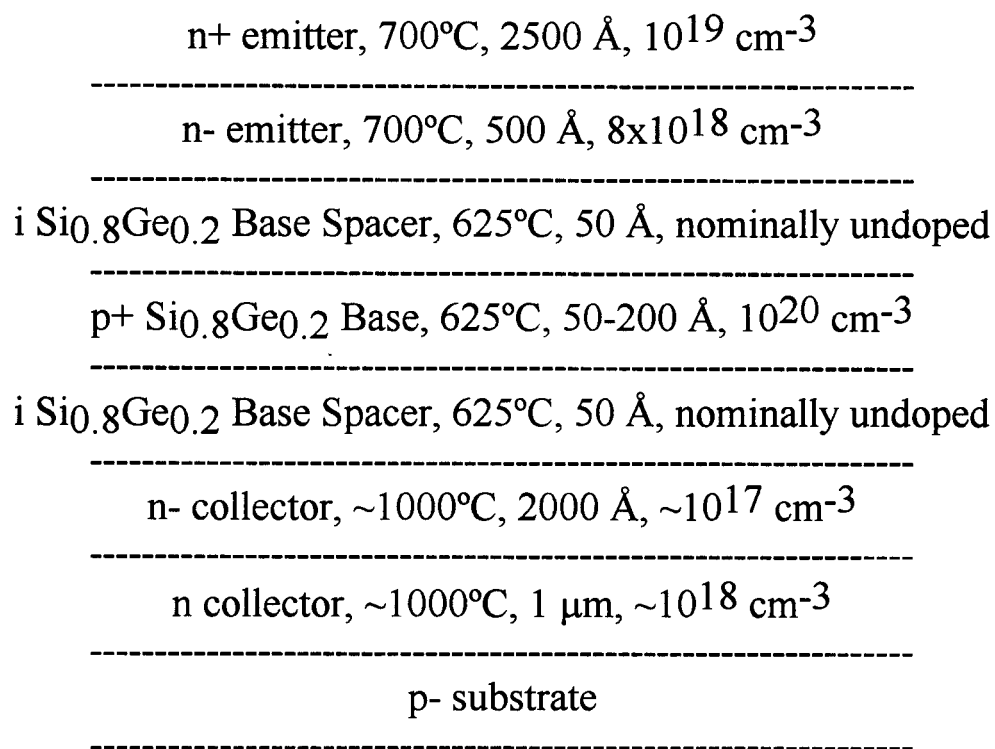


Figure 3.3: Growth sequence of a typical $\text{Si}_{0.8}\text{Ge}_{0.2}$ HBT used in this thesis.

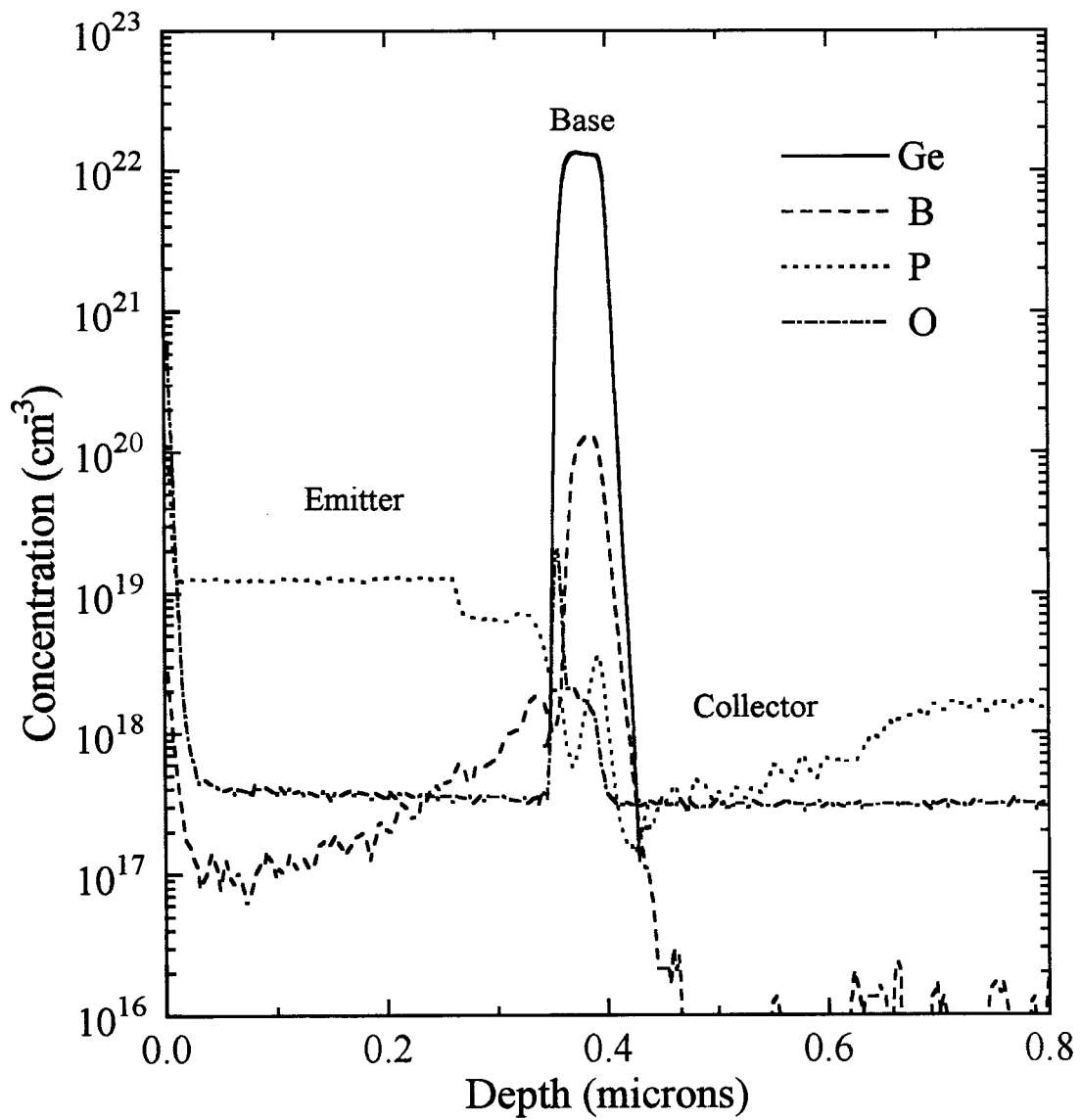


Figure 3.4: SIMS profile of a typical 300 Å thick Si_{0.8}Ge_{0.2} HBT used in this thesis. The doped thickness is ~200 Å.

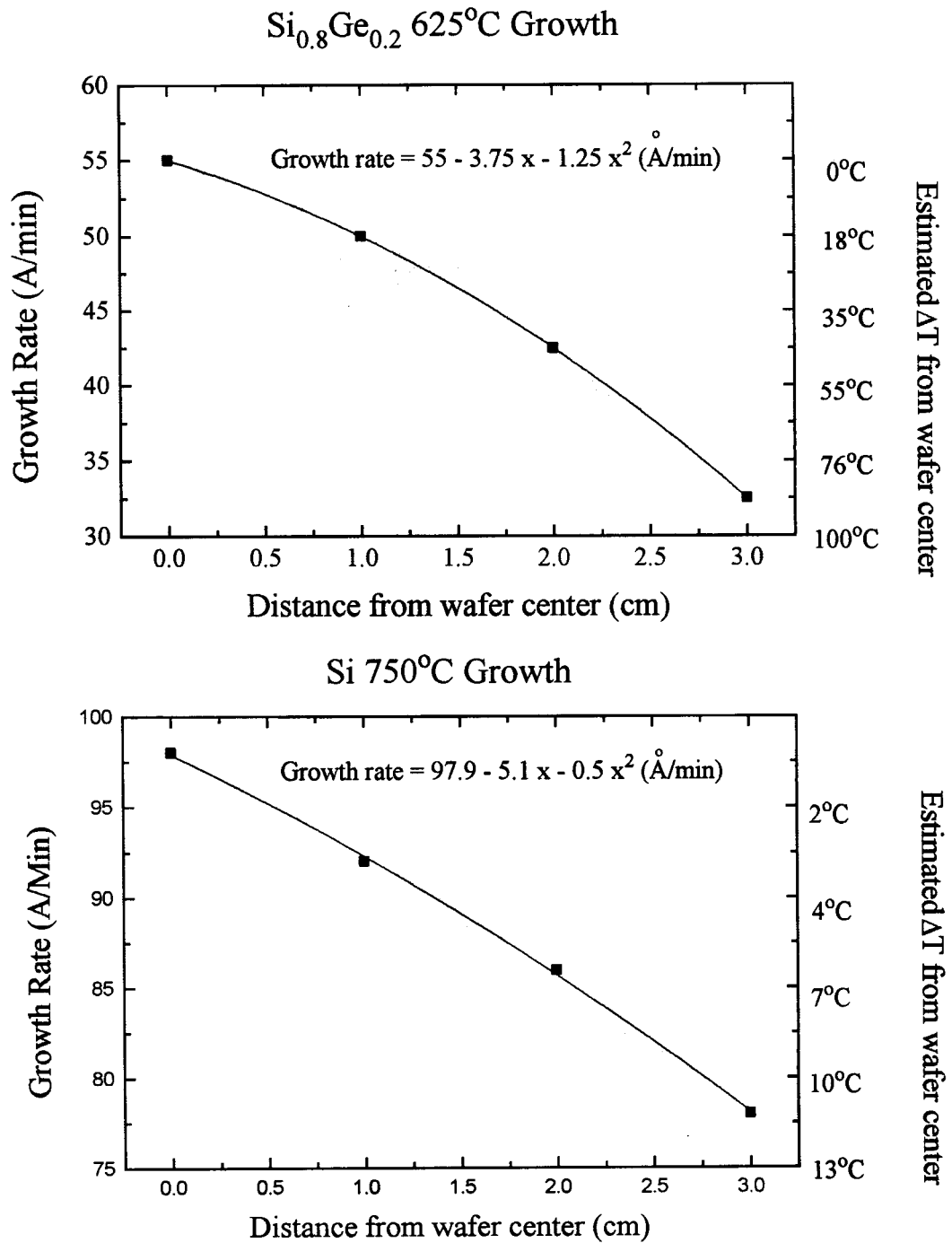


Figure 3.5: Growth rate nonuniformity in Princeton RTP chamber for 5 cm radius wafers. Growth activation energy for Si $E_A = 1.9 E_V$; SiGe $E_A = 0.38 E_V$. E_A data taken from [18]. x in growth rate formula is in cm.

the decrease in growth rate will also lead to an increase in germanium incorporation towards the edge of the wafer. This increase in germanium fraction has not been profiled.

3.2 The $\text{Si}_{1-x}\text{Ge}_x$ HBT Process

Following growth, the wafer is cleaved into $\sim 1\text{cm}$ by 1cm pieces for transistor fabrication. Once one has device epilayers, one needs a transistor "process" with which to fabricate the device. The process used for most of the devices in this thesis is as shown in Figure 3.6. It is a zero thermal budget, double mesa process designed to produce transistors with electrical properties identical to that of the as-grown wafers. This in contrast to manufacturable processes [8, 9, 23] which use postgrowth high temperature heat treatments which may affect the as-grown base doping profile.

As shown in Figure 3.6, the process begins with the definition of the emitter metal using liftoff. The emitter metal (500 \AA Cr, Ni, or Pt followed by 1500 \AA Au) is then used as an etch mask for a selective wet etch which etches the Si emitter not masked by the emitter metal but which stops on the SiGe base [24]. This selective wet etch (150 g KOH , $6\text{ g K}_2\text{Cr}_2\text{O}_7$, 150 ml n-propanol , $600\text{ ml H}_2\text{O}$, $\sim 100\text{ \AA/min}$ at room temperature, n-silicon) has been used with great success to fabricate devices with SiGe thicknesses of as thin as 150 \AA . Photoresist is then applied and patterned to protect the emitter metal and extrinsic base while etching through the SiGe base and lightly doped collector to contact the heavily doped collector. The n^+ collector is exposed using a SF_6 plasma etch and then the photoresist protecting the emitter is removed in acetone. Subsequently, the base and

Figure 3.5a: Define Emitter Area

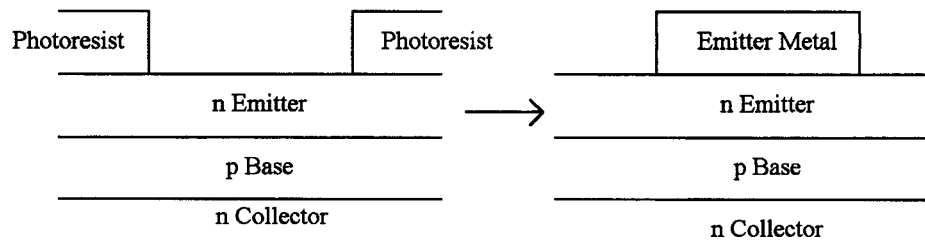


Figure 3.5b: Remove Si emitter using selective etch

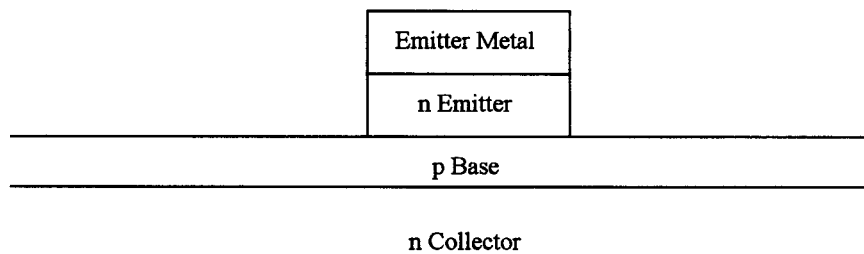


Figure 3.5c: Plasma Etch to Collector

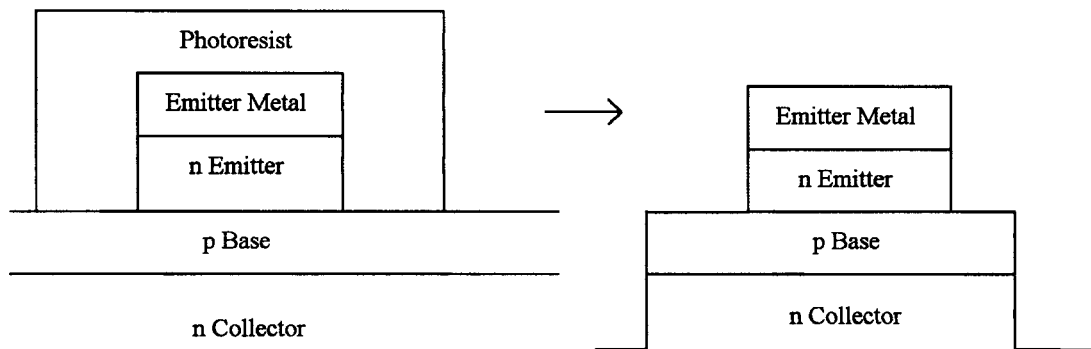


Figure 3.5d: Define Base, Collector Metals

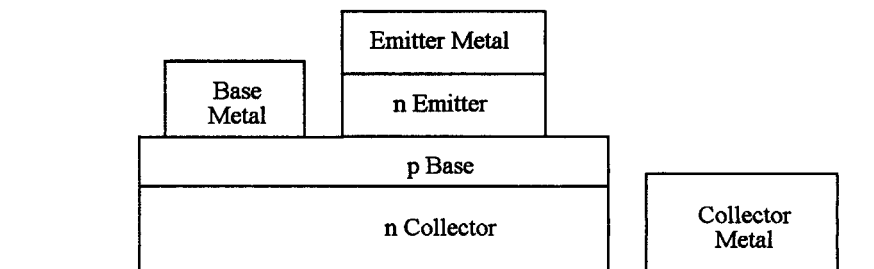


Figure 3.6: Double mesa transistor process used to fabricate SiGe HBTs.

collector contacts (500 Å Ti followed by 1500 Å Al) are evaporated by liftoff. No forming gas contact anneals were used for any of the devices in this thesis.

3.3 Summary

This chapter has served as an introduction to the growth system and process used to fabricate the HBTs used in this thesis. Wafer to wafer reproducibility was discussed.

Si_{1-x}Ge_x HBTs in the Real World

4.1 Introduction

The discussions of electrical device behavior have, up until now, focused primarily on how SiGe transistors should ideally behave. In practice, however, there are many important complications. The three issues which this chapter addresses are the scaling of transistor collector saturation current with varying base width, the non-ideal base currents of this thesis's devices, and the problems of boron diffusion in SiGe HBTs. The concept of non-ideal base currents is important to understand the research discussed in Chapter 7. Boron diffusion is important for understanding the importance of the results obtained in Chapter 7.

4.2 Bipolar Transistor Experiments

While the equations presented in Chapter 2 for collector saturation current are relatively simple, constructing meaningful experiments by varying the parameters W_B , N_B and germanium fraction in a university setting can be quite challenging. The germanium fraction affects $n_{i,(base)}^2$ through E_G , $SiGe$ as well as through $N_{C,SiGe}$ and $N_{V,SiGe}$. Problems arise because the SiGe CVD growth rate and hence W_B is a strong function of both germane flow and temperature [21]. Hence W_B , which is a difficult parameter to measure without TEM or SIMS, will vary with Ge content, assuming a fixed growth time. Changing growth rates associated with changing Ge content and changing temperature will also affect the boron incorporation which affects N_B [25, 26]. In addition, in heavily doped bases one must consider doping-induced bandgap narrowing in addition to Ge-induced bandgap narrowing [27]. Hence the easiest parameter to vary is W_B by simply keeping all the flow and temperature parameters constant and adjusting the growth time of the doped base. From Equation 2.2, one would expect that doubling the base thickness by doubling the growth time would lead to a factor of two decrease in transistor collector saturation current.

Figure 4.1 shows collector currents for 20% Ge, 10^{20} cm^{-3} boron doped bases with doped base thicknesses of roughly 50, 100, and 200 Å. The collector saturation currents decrease by a factor of 1.5 between the 50 and 100 Å bases and 1.6 between the 100 and 200 Å bases. Since each sample has 50 Å undoped SiGe layers surrounding the doped SiGe base (the importance of which will be discussed in Chapter 4), the total SiGe thicknesses for the samples are 150, 200, and 300 Å. Figure 4.2 shows SIMS of the Ge profiles which confirms the expected SiGe thicknesses. This data indicates, within the errors in base thickness measurement and doping concentration, that standard drift and

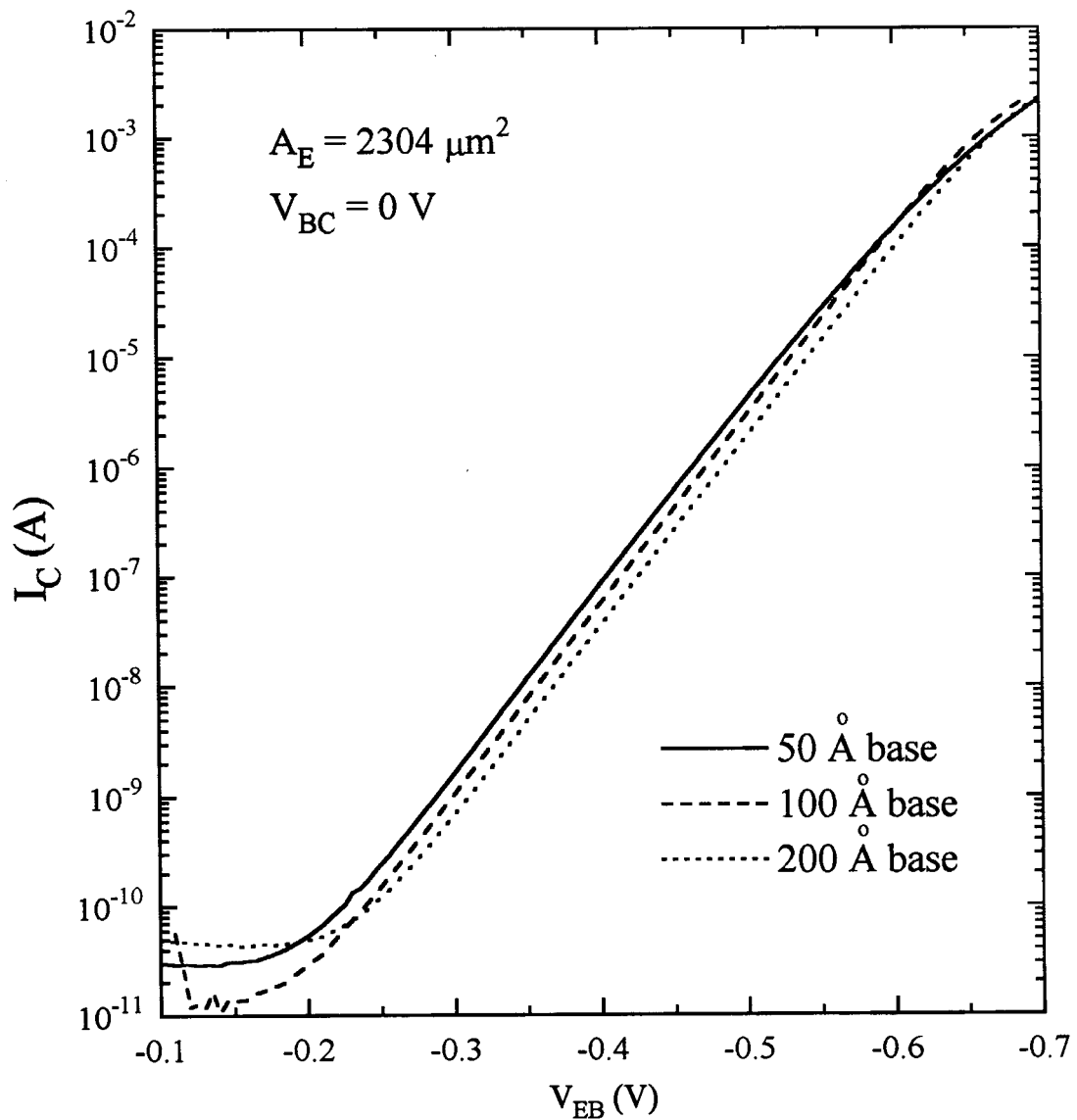


Figure 4.1: Collector current characteristics of $\text{Si}_{0.8}\text{Ge}_{0.2}$ HBTs with doped base widths of 50, 100, and 200 Å.

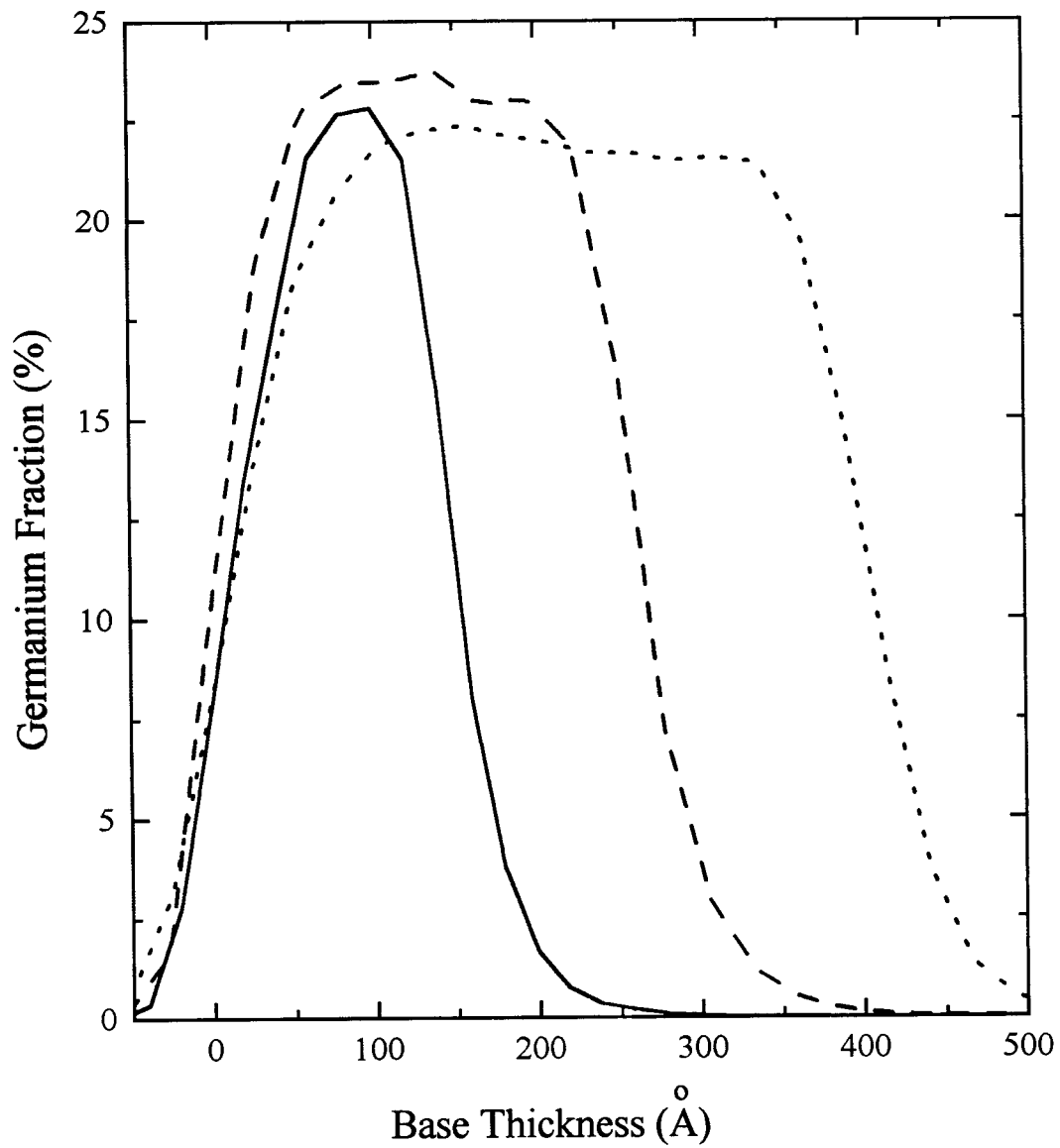


Figure 4.2: SIMS of SiGe bases with expected SiGe thicknesses of 150, 200, and 300 Å. Measured FWHM are 130, 255, and 380 Å.

diffusion models of minority carriers in the base of an HBT are qualitatively applicable to SiGe bases for modelling DC currents of bases with thicknesses down to at least 50 Å. This is relatively important because interesting transistor effects have been predicted to occur for base thicknesses on the same order of magnitude of the mean free path of a minority carrier in the base [28-35].

4.3 Non-Ideal Si_{1-x}Ge_x HBT Base Currents

The first issue to be addressed is that of the non-ideal base currents of the devices used in this thesis. In modern textbook discussions of bipolar transistors, the dominant component of base current is recombination in the neutral base, neutral emitter, or at the emitter contact. Thus the base currents, as well as the collector currents, should be "ideal" and have a voltage dependence of $e^{qV/kT}$. Hence, at room temperature, both the collector and base currents should have slopes of ~ 60 mV/decade. This gives a constant transistor current gain over several orders of magnitude in current on a Gummel Plot, as shown in Figure 2.6. Ideal sources of base current are minority carrier neutral base recombination or injection of holes from the base into the emitter.

The base current caused by holes being injected into the emitter is

$$J_{B,emitter} = \frac{qD_p n_{i,emitter}^2}{N_D L_p} e^{qV_{BE}/k_B T} \quad [4.1]$$

for emitter thicknesses greater than the diffusion length of holes in the emitter. N_D is the emitter doping and D_p is the diffusion length for holes in the emitter.

However, in the real world, base currents can come from many non-ideal sources such as unpassivated surfaces [29] and traps in the emitter-base depletion regions [36-39]. Both of these are sources for minority carrier recombination and can give rise to base currents with a voltage dependence of $e^{qV/nkT}$ with $n > 1$. The first source of non-ideal base current, that of unpassivated surfaces, is process dependent. Unpassivated surfaces of p-n junctions can lead to excess diode leakage currents. Transistors fabricated using a double mesa process such as those in this thesis will always suffer from it.

The second case, that of traps in the emitter-base depletion region, is dependent on high quality epitaxial layers and on the doping concentrations in these layers. If traps exist in heavily doped ($>10^{19} \text{ cm}^{-3}$) emitter-base depletion regions, electrons from the emitter and holes from the base can tunnel into the forbidden gap in the depletion region and recombine at trap sites there, as shown in Figure 4.3. Hence, to eliminate this source of non-ideal base current, the emitter-base depletion region should be kept as free from contamination as possible. While standard textbook descriptions of depletion region recombination is not related to tunneling, traps are important in the devices used in this thesis because of the high emitter and base doping concentrations.

Figure 4.4 shows typical Gummel characteristics for a SiGe base HBT grown with a silane emitter. Note that the ideality factor of the base current is ~ 2 . It was thought for the substantial part of this thesis work that such currents originated from recombination at the unpassivated surfaces of the emitter-base depletion region. Figure 4.4 also shows the Gummel characteristics for a transistor grown with a DCS emitter instead of a silane emitter. The transistor was fabricated using the same unpassivated double mesa structure as the silane emitter. Note that for an identical, unpassivated transistor structure, the base current in the DCS emitter transistor has an n factor of 1.5. The fact that the base currents of a transistor with a DCS emitter are more ideal than the silane emitter

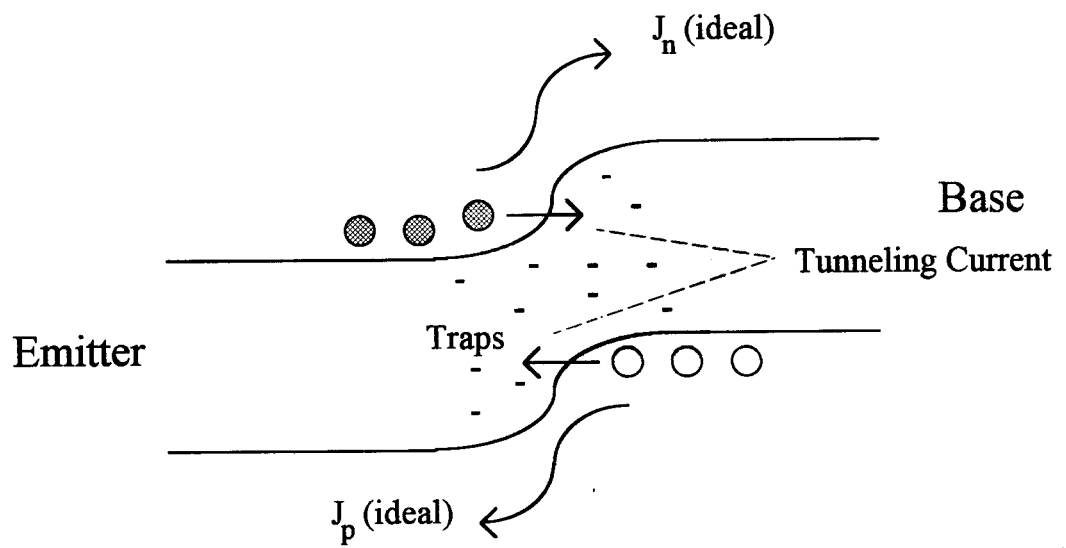


Figure 4.3b: Tunneling currents.

Figure 4.3: Origin of trap related non-ideal base currents.

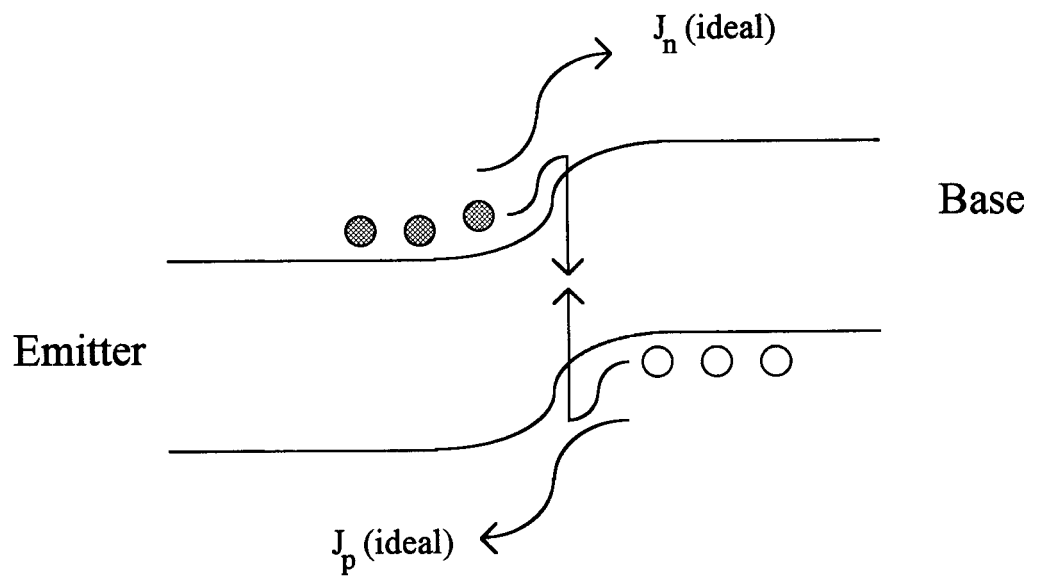


Figure 4.3a: Usual recombination currents

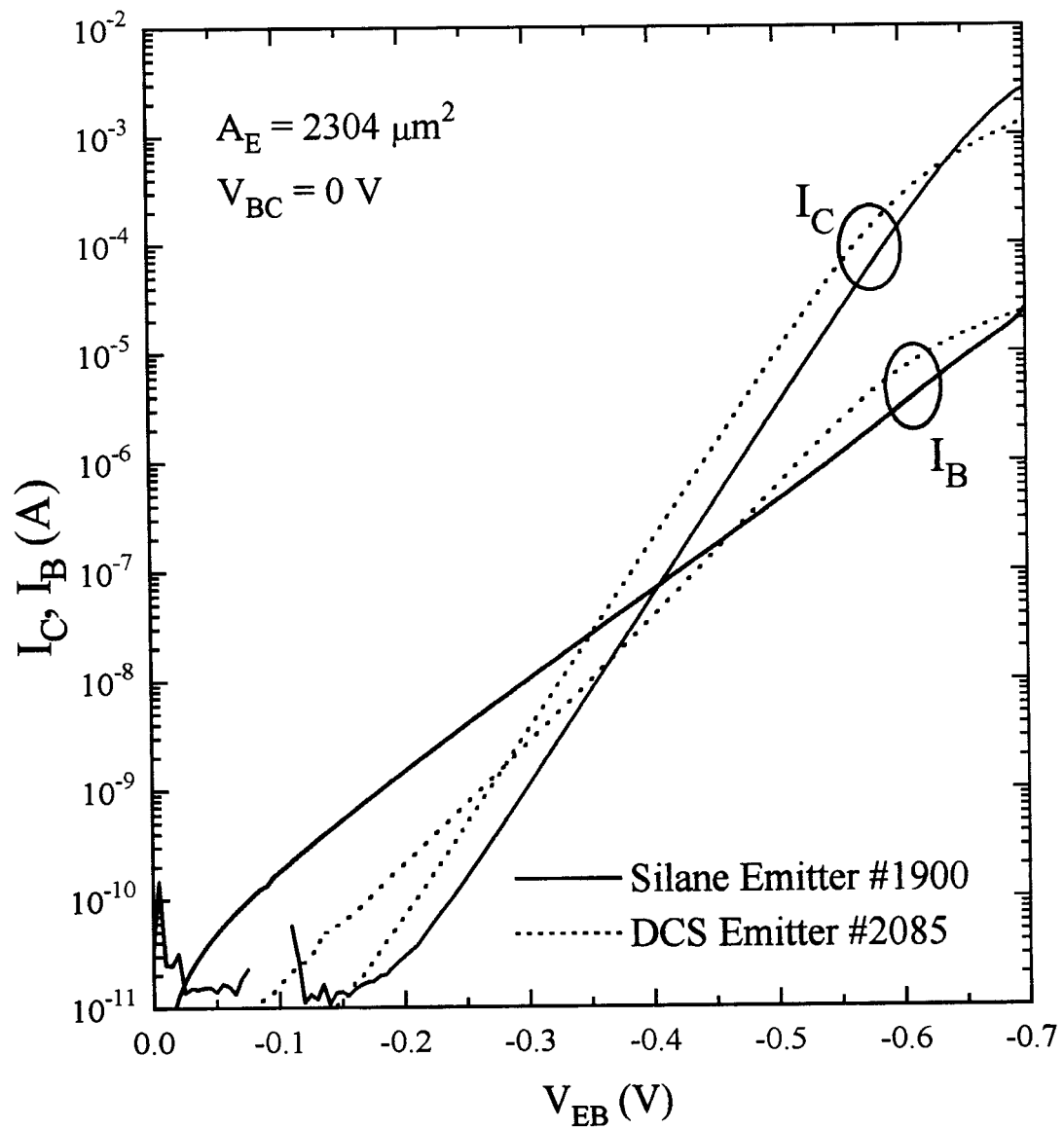


Figure 4.4: Common base characteristics of SiGe HBTs grown using both silane and DCS emitters.

transistor's base currents, despite the same double mesa structure, indicates that there is a more important base current mechanism at play which was not anticipated. (The collector saturation currents for both transistors are different due to different base germanium fractions, doping levels, and base widths.)

Figure 4.5 shows SIMS profiles of the base region of Figure 3.4, to illustrate the transition from SiGe base to Si emitter grown with silane. Figure 4.6 shows SIMS profiles for a detail of a SiGe base with a Si emitter grown using DCS. It is readily apparent that the fundamental difference between the silane and DCS transistors is the existence of a $\sim 10^{19} \text{ cm}^{-3}$ oxygen spike at the emitter-base junction in the silane emitter transistor which is not present in the DCS emitter transistor. This oxygen spike is presumably caused by changing the silicon precursor gas from DCS to silane following the base growth. While this gas switch was accomplished by turning off the DCS source and turning on silane simultaneously with no time delay, this process results in oxygen contamination precisely in the location where it will create the most electrical damage (Figure 4.3). While switching from DCS to silane and back to DCS is not uncommon in silicon bipolar epitaxy [40], at this time it is unknown whether this oxygen incorporation is a fundamental physical growth effect perhaps due to some change in the Si surface during the switch from SiGe base to silane grown emitter or simply due to an oxygen problem with the reactor. This may be due to limitations in the reactor gas supply, where it was unfortunately not possible to flush the silane supply line immediately before the silane deposition. It is disappointing to note that all the transistor epitaxial layers to be discussed in Chapters 6 and 7 of this thesis were grown with silane emitters. Consequently, these transistors suffer from higher non-ideal base currents than would result simply from the lack of surface passivation.

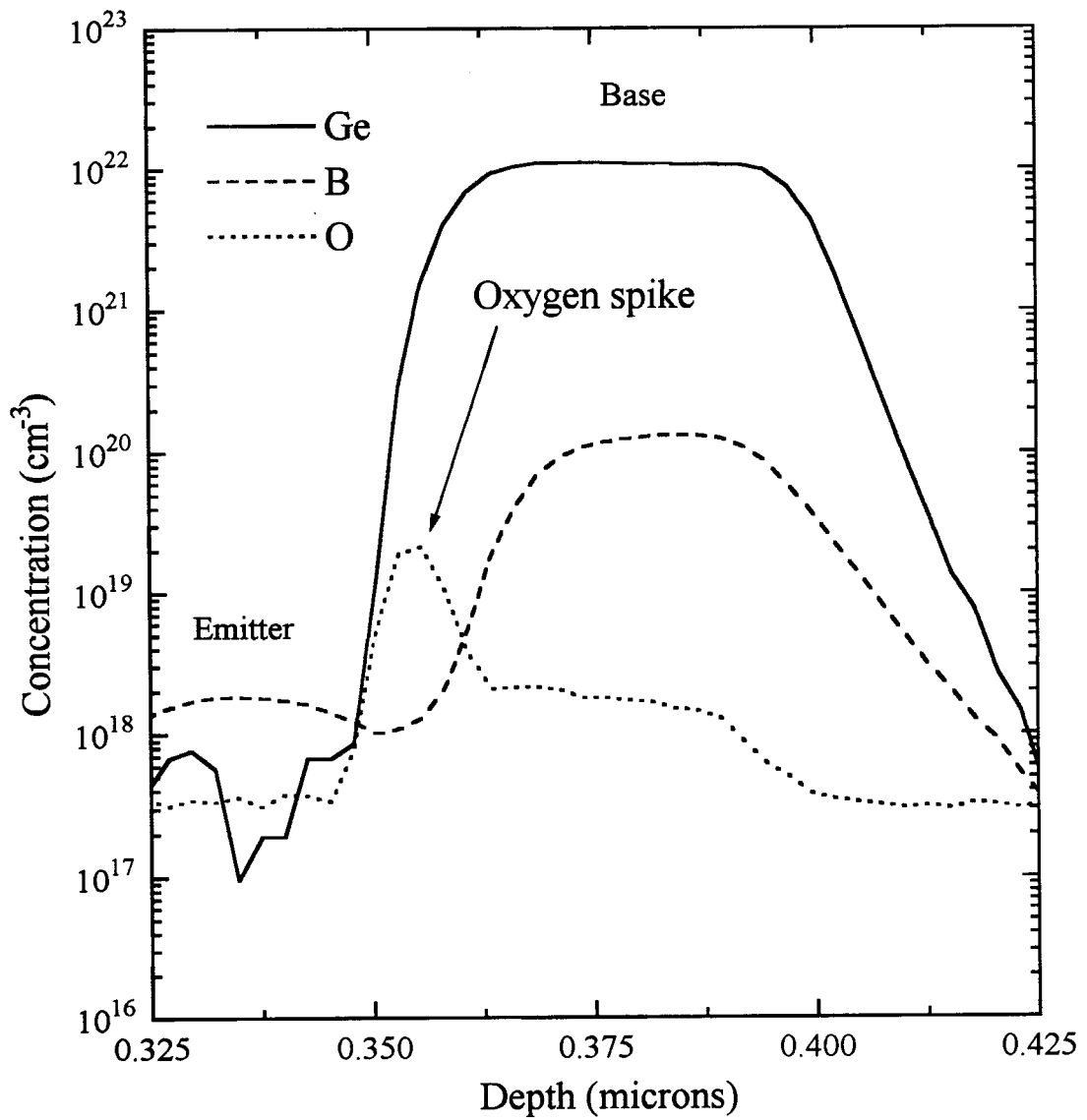


Figure 4.5: SIMS profiles showing the composition of a $\text{Si}_{0.8}\text{Ge}_{0.2}$ base grown with a silane emitter.

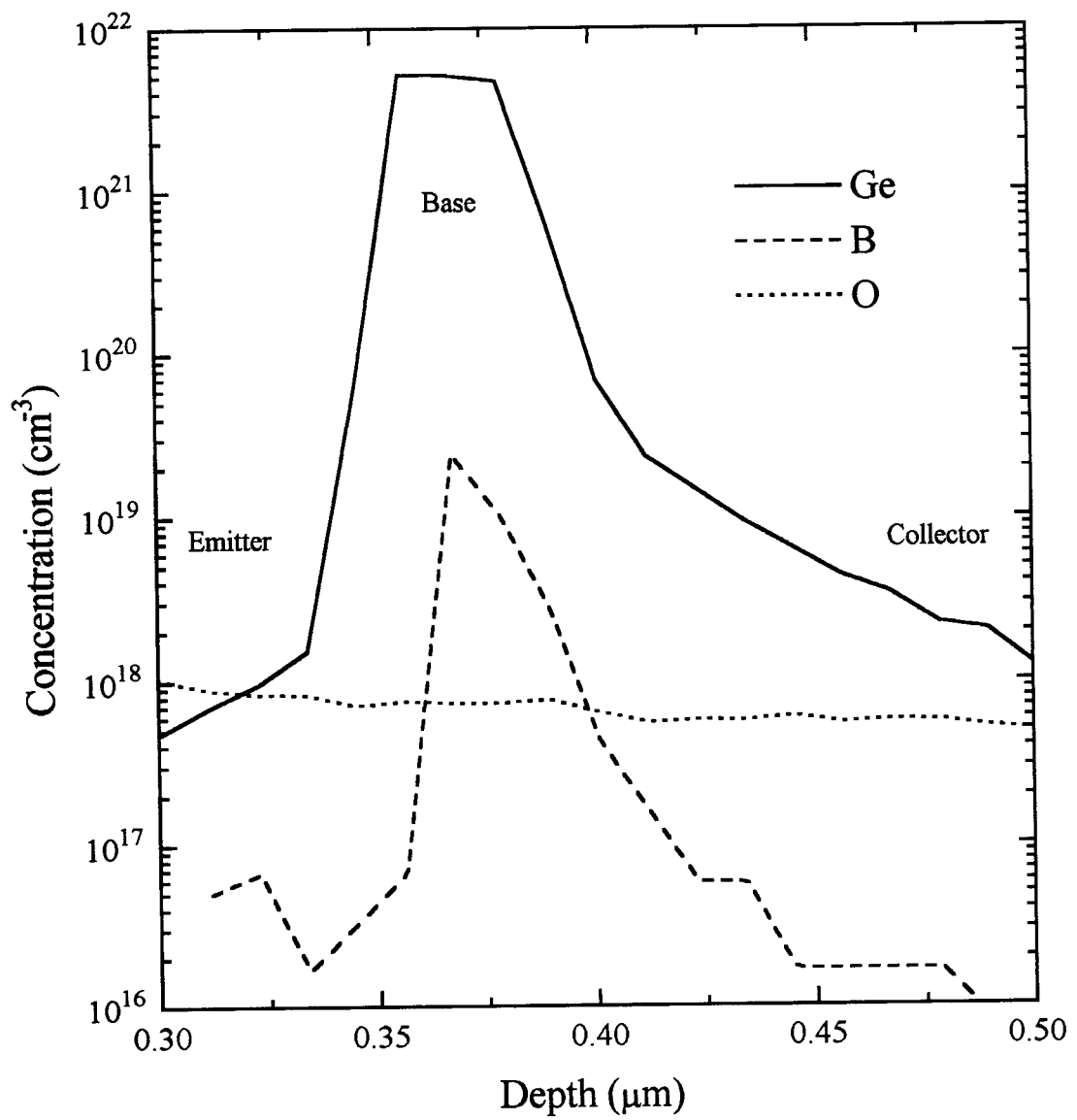


Figure 4.6: Detail of a SiGe base grown with a DCS emitter.

4.3.1 Quasi-Ideal Base Current HBTs with Heavily Doped Emitters

While HBTs grown with DCS emitters have more ideal base currents than devices grown with silane emitters, HBTs grown with DCS emitters incorporating high emitter oxygen concentrations have near ideal base current characteristics. Unpassivated surfaces and high *emitter* oxygen concentrations do not necessarily preclude a device from having near-ideal base current characteristics. Figure 4.7 shows characteristics of two different double mesa, high emitter oxygen concentration transistors whose base current ideality factors are ~ 1.2 . Hence the base currents are more ideal compared to transistors grown using DCS emitters as shown in Figure 4.8. These transistors were grown using a DCS emitter process which achieved high emitter n-type doping to reduce the emitter series resistance and emitter contact resistance for high frequency transistor operation. In addition, high oxygen concentrations were unexpectedly incorporated into the emitter in these devices.

It may be argued that the near-ideal base currents are due to a high level of recombination in the neutral emitter. However, these near-ideal base currents were discovered by accident and only much later when SIMS was performed did the possible reasons for ideal behavior become apparent. In any case, these base current effects were not examined in detail since the high frequency project for which they were grown was cancelled immediately following the growth of these wafers.

The growth of heavily doped n-type crystalline silicon by CVD is problematic; phosphorus incorporation at low temperatures and low pressures using silane and DCS is limited to $\sim 10^{19} \text{ cm}^{-3}$ as shown in Figure 3.4. Increasing phosphine flow during silane growth leads only to a decrease in growth rate with no increase in doping level [41]. 10^{20} cm^{-3} n-type doping concentrations are readily achieved in SiGe, however [42]. The only viable method to achieve 10^{20} cm^{-3} phosphorus levels in crystalline silicon with

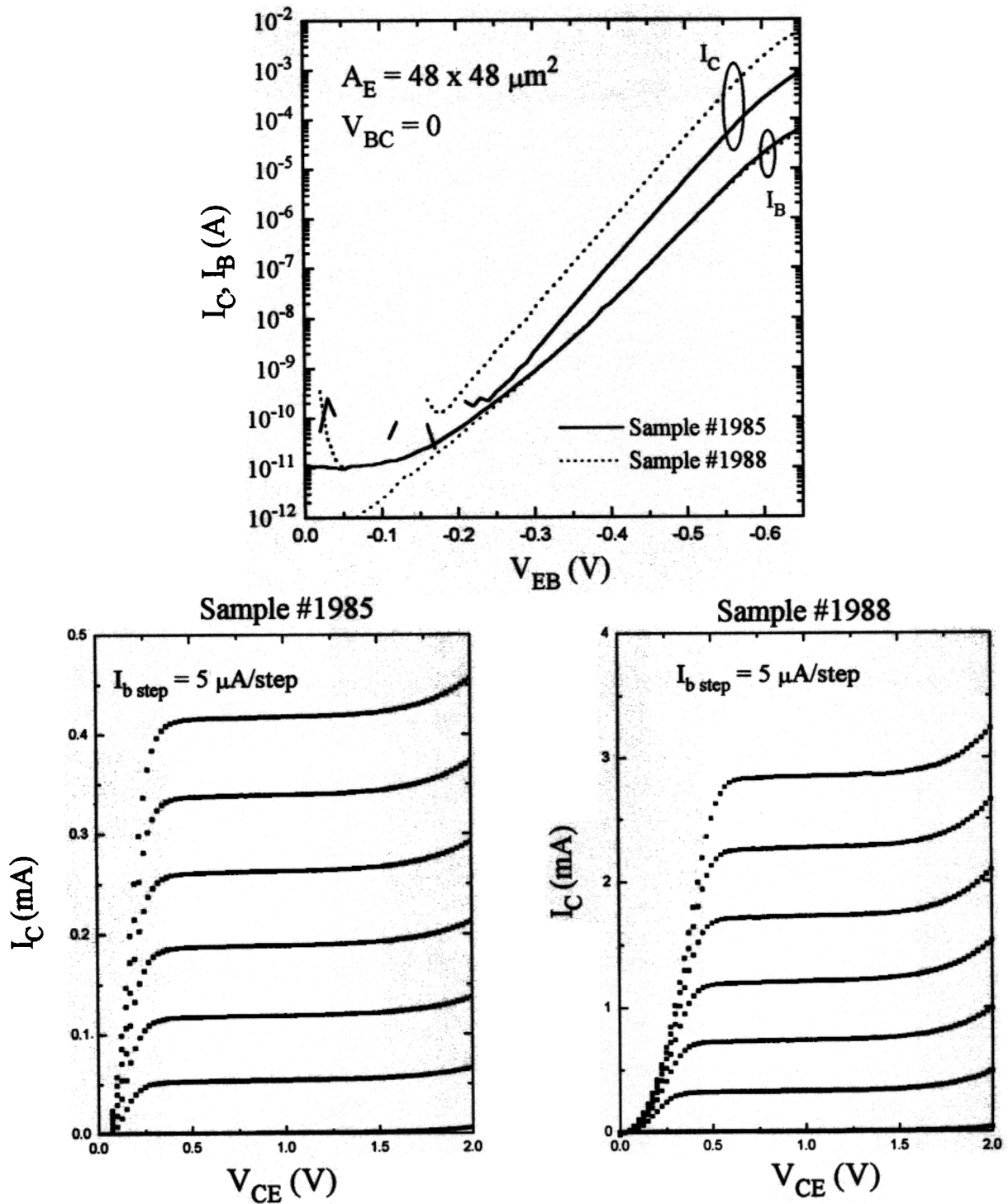


Figure 4.7: Transistor characteristics of double-mesa SiGe HBTs with high oxygen concentrations in the emitter and ideal base current characteristics.

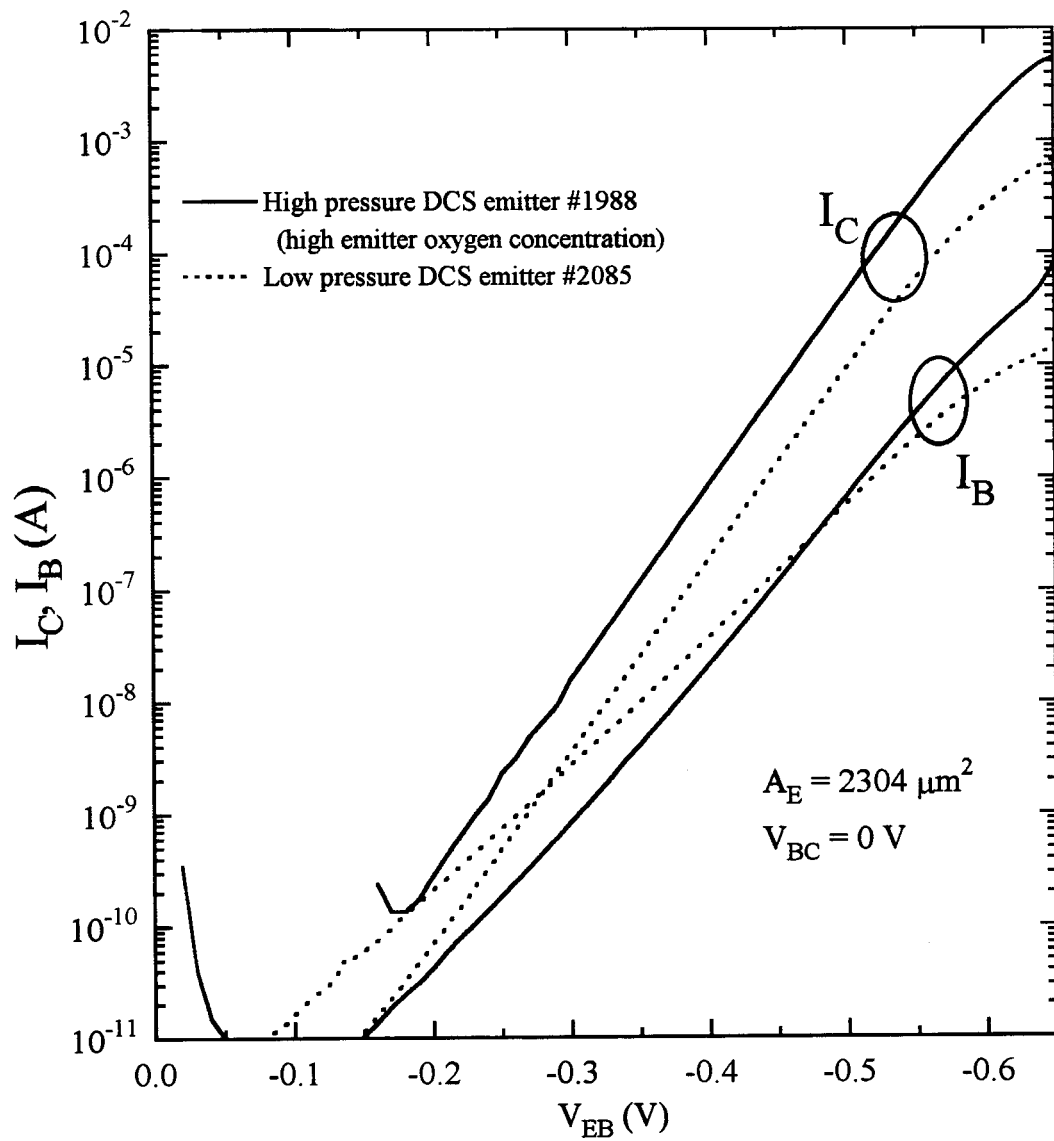


Figure 4.8: Comparison of Gummel plots from transistors with different DCS emitters.

outdiffusion, even at 25 Å length scales. It is, however, important to exercise some caution in using these measurements. As one moves towards the edge of the 4 inch wafer, the wafer growth temperature is lower, leading to a decreased growth rate. Hence spacer thicknesses as well as doped base thicknesses decrease slowly towards the edge of the wafer.

Figure 4.17b shows characteristics of a transistor fabricated from pieces half way between the center and edge of a wafer with 50 Å spacers. Devices fabricated from material from the center of this wafer are known not to be outdiffused, as shown in Figure 4.17a. One can see a marked difference in the common emitter characteristics due to the onset of outdiffusion. Outdiffused common emitter curves similar to those of Figure 4.17b have been previously demonstrated [48]. Hence just because devices from the wafer center are not outdiffused does not necessarily imply that devices from the edge are not outdiffused because of the thinner spacer layers near the edge. The researcher using this reactor's epi material needs to be aware of the fact that wafers grown in this reactor can have varying device characteristics due to thickness nonuniformities.

To get an idea of the spacer thickness required to prevent outdiffusion, as well as of the nonuniformity inherent in Princeton's RTCVD growth chamber, Figure 3.5 plots growth rate as measured by TEM vs. distance from the center of a wafer for two different growth conditions. Note that a growth wafer has a radius of 5 cm. Hence any device fabricated from material halfway between the center and the edge of the wafer will have $\text{Si}_{0.8}\text{Ge}_{0.2}$ thicknesses ~35% and Si thicknesses ~20% less than that of devices fabricated from material at the center.

Hence the device from Figure 4.17b has ~ 35 Å spacer thicknesses, in contrast with the wafer from Figure 4.17a, which has spacer thicknesses of ~50 Å, even though both devices came from the same wafer.

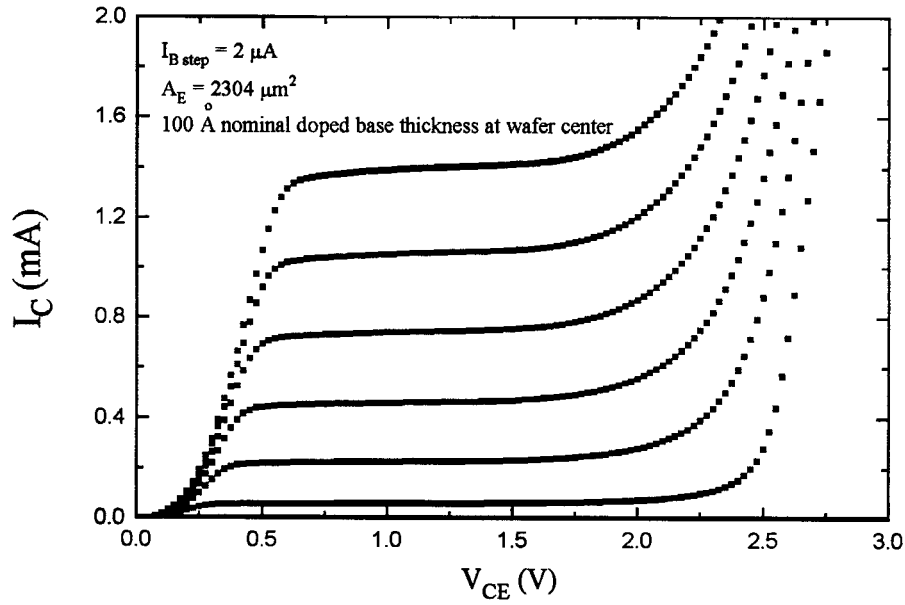


Figure 4.17a: Device from wafer center

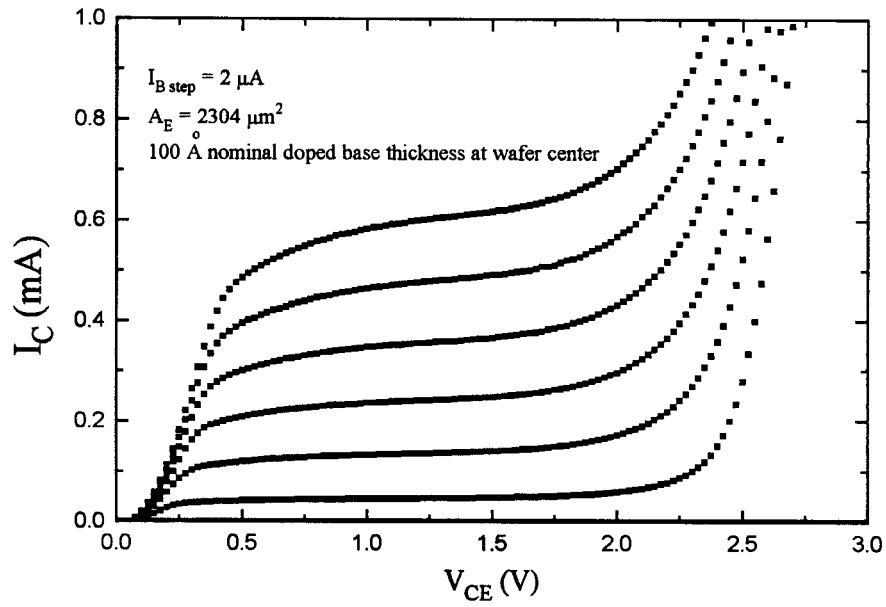


Figure 4.17b: Device from piece half way between wafer center and edge

Figure 4.17: Common-emitter characteristics from the center and halfway to the edge of the same $\text{Si}_{0.8}\text{Ge}_{0.2}$ HBT wafer.

One may conclude from this data and the data presented in Figure 4.16 that, in order to correctly predict the effects of outdiffusion on the transistor characteristics of $\text{Si}_{0.8}\text{Ge}_{0.2}$ devices, one needs to understand, and model correctly, the consequences of boron outdiffusion on device performance down to a level of tens of angstroms.

4.5 A Final Note

The common-emitter characteristics of the transistors used in this thesis display large ($\sim 0.5\text{V}$) V_{CE} offset voltages. This is due to the large collector series resistance due to the low subcollector n-type doping and the high collector contact resistance. These resistances seriously limit the amount of forward base-collector current at fixed base-collector forward bias required to drive the transistor into saturation.[52] Large V_{CE} offset voltages of $\sim 0.5\text{ V}$ have also existed in previous double-mesa Princeton HBTs fabricated using lightly doped subcollectors, however. [15]

Before concluding this section it is necessary to note that undoped spacer layers surrounding SiGe is yet another tradeoff in device performance vs. materials science. While these spacers are necessary to prevent outdiffusion, they consume total base critical thickness without contributing to a reduction of base sheet resistance because they are not doped. Hence one cannot use arbitrarily large spacer thicknesses due to critical thickness limitations. Enhancing SiGe critical thickness would be desirable to relax these tradeoffs. This topic will be addressed in Chapters 5 and 6. Reducing boron diffusion will be discussed in Chapter 7.

4.6 Summary

This chapter has served to introduce the real world problems a SiGe HBT researcher faces due to process and equipment constraints. The subject of non-ideal base currents was focused on using an investigation of three different emitter structures. SiGe HBTs with heavily-doped single-crystalline phosphorus emitters containing a background oxygen concentration of $\sim 10^{20} \text{ cm}^{-3}$ were shown to have quasi-ideal base current characteristics despite an unpassivated double-mesa structure.

The degradation in SiGe HBT electrical characteristics due to boron outdiffusion was established. The chapter finished with a discussion of the experimental limitations caused by SiGe thickness non-uniformities due to wafer temperature variations.

Introduction to Carbon in Si and $\text{Si}_{1-x}\text{Ge}_x$

5.1 Motivation for Carbon in Si-based Alloys

The finite critical thickness of SiGe causes transistor design tradeoffs between base thickness, spacer thickness, Ge fraction, and base doping concentration. Loosening this critical thickness limitation would be a desirable step forward for SiGe HBTs as well as for other devices built from SiGe. The fact that germanium is a larger atom than Si gives rise to the strain in SiGe which limits critical thickness. A substitutional carbon atom, however, is both isoelectronic and smaller than both Si and Ge. Diamond has a lattice parameter of 3.56 Å compared to 3.57 Å for silicon or 3.57 Å for germanium. Hence incorporating substitutional carbon atoms into $\text{Si}_{1-x}\text{Ge}_x$ alloys, forming the new alloy $\text{Si}_{1-x-y}\text{Ge}_x\text{C}_y$, would be expected to reduce the strain in $\text{Si}_{1-x}\text{Ge}_x$. Previous workers have shown that 1% C in Si compensates the strain of 8.3-10% Ge [53, 54]. Hence a typical 20% Ge HBT would be lattice matched to a Si wafer if it contains approximately 2% C. This material would be desirable from a device point of view since the critical thickness constraint limiting spacer thickness and base width would now be lifted.

5.2 Early Work on Carbon in Silicon

However, from previous research on C in Si, one would not expect encouraging results from C in SiGe. The fundamental problem associated with carbon in Si is that while Ge is completely miscible in Si, the solid solubility of C in Si is $4 \times 10^{17} \text{ cm}^{-3}$ at the melting point of silicon [55]. SiC, the stable form of C in Si, will tend to form at concentration levels higher than this. As a result of the low solubility of C in Si, workers prior to the early 1990's regarded carbon as a contaminant.

Reviews of older work on carbon center on carbon in as-grown silicon wafers [56] and focus on measuring the diffusion coefficient of carbon in silicon and the effects of high temperature heat treatments on carbon in silicon. Gosele reviewed work on the interaction of point defects with carbon [57]. Early work on C in Si centered on the measurement of the effect of carbon on the silicon lattice constant [58], of the solubility of carbon in silicon [59] and of the diffusivity of carbon in silicon [60]. It was shown that 10^{18} cm^{-3} carbon atoms in silicon wafers form SiC precipitates following a 900°C , 160 minute anneal [61]. Research on the effects of carbon on electrical device properties showed that 10^{17} cm^{-3} carbon atoms in as-grown wafers caused degradation of diode breakdown voltages due to SiC precipitation following 1300°C anneal for 119 hours [62]. A review of the effect of $5 \times 10^{16} \text{ cm}^{-3}$ carbon concentrations on electrical devices focused on the degradation in device performance caused by high temperature (1200°C , 15 hours) processed induced "swirl" defects [63].

[42], and no SiGe strain relaxation effects due to the small boron atoms (Chapter 5), the collector saturation current of Sample #1985 should be half that of Sample #1988. As shown in Figure 4.7, the actual difference in saturation currents is a factor of seven, indicating that, not surprisingly, heavy doping effects need to be considered in these transistors. The base boron concentration is $6 \times 10^{20} \text{ cm}^{-3}$ ($\sim 1\%$), yet this transistor still has $\beta \sim 20$!

Considering the high boron fractions and high emitter oxygen concentrations, these devices are not "normal" SiGe transistors. They are actually $\text{Si}_{1-x-y}\text{Ge}_x\text{B}_y$ alloy transistors with high base current ideality factors. The fact that the base current is so ideal despite the unpassivated surfaces in the double mesa process probably has something to do with the high oxygen concentrations in the lightly doped emitter which would reduce the lifetime of holes in the emitter. However, the fact that the base current of the transistor with oxygen in the emitter is actually less, at low V_{BE} , than the base current of the DCS transistor is puzzling. The oxygen doped silicon may also serve as hole blocking layer, as in the case of polycrystalline emitter bipolar transistors. The ideal base currents could also be due to neutral base recombination caused by the heavily doped boron base.

Any attempt to quantify this data without further experiments would be purely speculative especially since the oxygen contamination of the films was not known when these experiments were performed. The author doesn't believe in quantitative experiments which consist of only two growth wafers, especially when the wafers were not grown to optimize the examination of an effect which was not known to be occurring.

The high germanium and boron contents in these films are not all that outrageous for research purposes, however. Novel SiGe HBTs have been demonstrated which use up to 57.5% Ge fractions and 10^{20} cm^{-3} base doping levels [45]. The use of $4 \times 10^{20} \text{ cm}^{-3}$ SiGe HBT doping levels have been proposed [45] and SiGe HBT devices which utilize

$2 \times 10^{20} \text{ cm}^{-3}$ base doping levels have been used to demonstrate record high frequency transistor performance [46].

In the Princeton chamber, the growth rate of 10^{19} cm^{-3} phosphorus concentrations at 700°C using DCS at 6 torr is 17 \AA/minute . The growth rate of 10^{20} cm^{-3} phosphorus concentrations at 700°C with DCS at 250 torr using this method is 57 \AA/minute . Hence a growth rate enhancement of 3.3 was achieved, as would be expected from previous work [43].

4.4 Boron Outdiffusion in SiGe HBTs

In addition to the finite SiGe critical thickness, another major constraint related to SiGe HBTs is that of boron diffusion from the heavily doped p-type SiGe base into the Si n-type emitter and collector. The key problem results from the fact that a 10^{20} cm^{-3} boron doped SiGe base is doped 1-2 orders of magnitude higher than the n-type emitter and ~ 3 orders of magnitude higher than the n-type collector, as seen in Figure 3.4. Diffusion of boron out of the SiGe base will therefore turn the formerly n-type Si emitter and collector p-type, as shown in Figure 4.13. This boron "outdiffusion" from SiGe into Si leads to quite dramatic changes in SiGe HBT electrical characteristics because of the presence of the Si/SiGe heterojunctions surrounding the base. The causes and consequences of this boron outdiffusion on the electrical characteristics of the device have been extensively studied and modeled [15, 47-51].

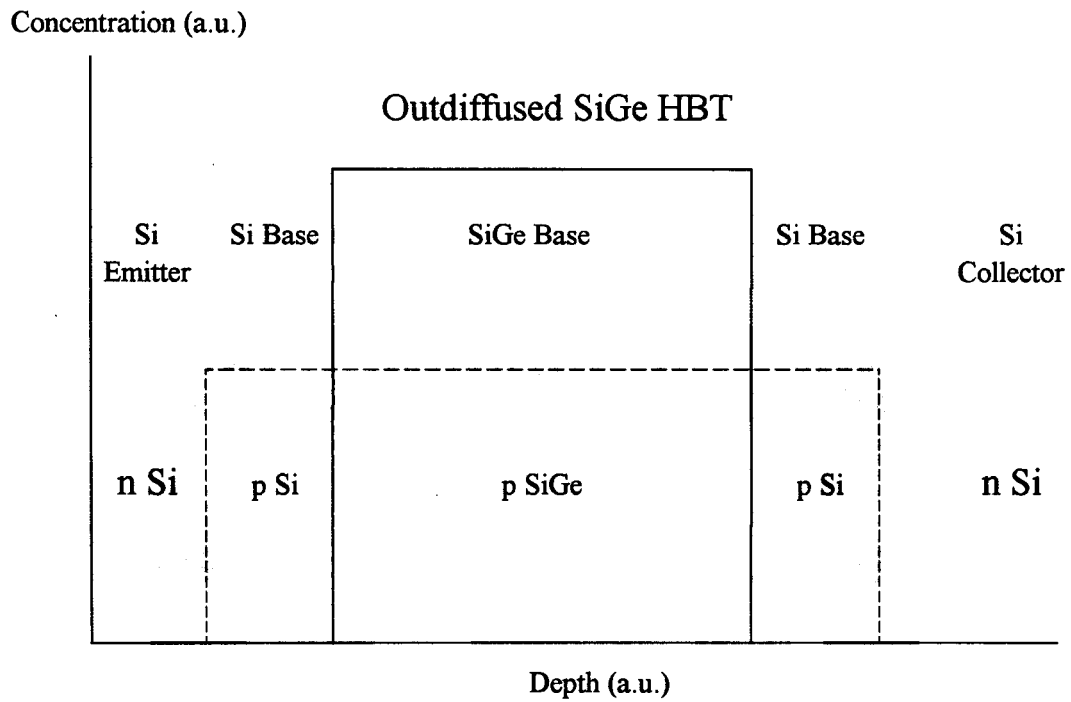
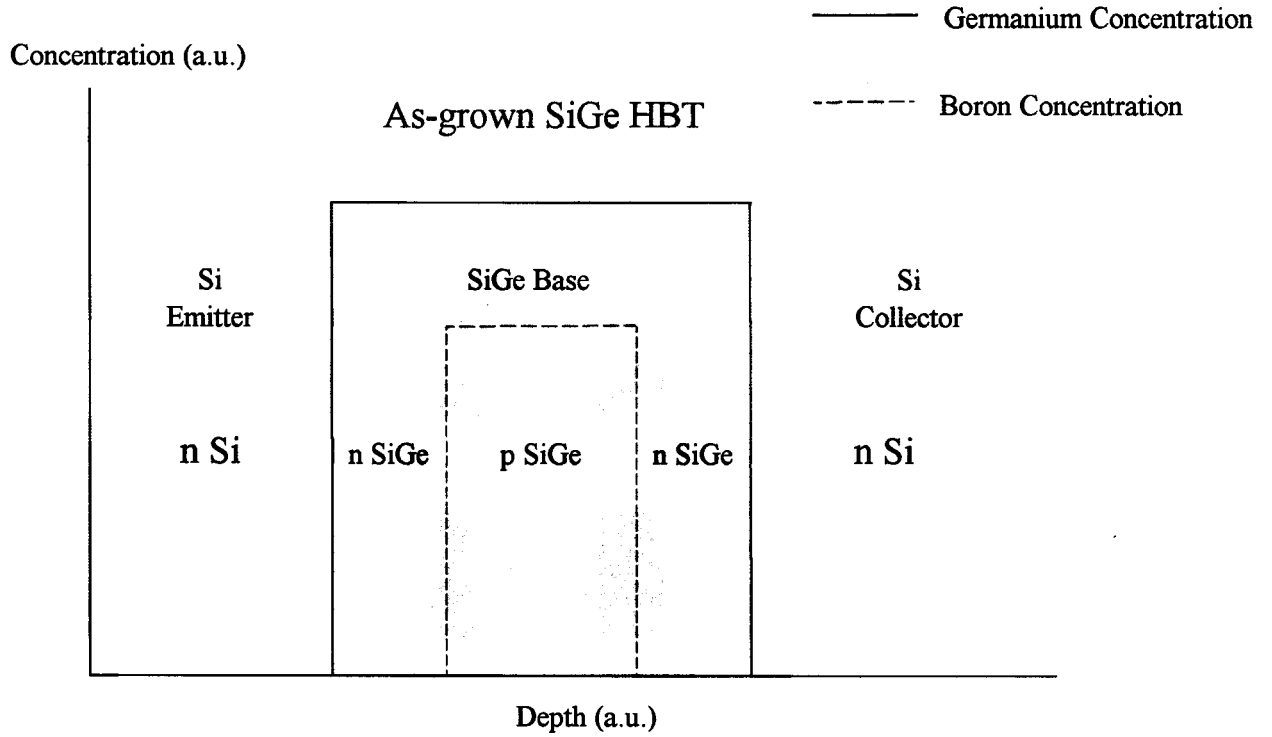


Figure 4.13: Comparison of the boron profile of a SiGe HBT with spacers with that of an outdiffused SiGe HBT.

4.4.1 Outdiffusion Theory

Figure 4.14 shows the conduction band of an outdiffused SiGe HBT along with that of an as-grown SiGe HBT. The silicon collector and emitter surrounding the SiGe have been turned p-type leading to the formation of barriers on either side of the SiGe because of the larger bandgap in Si compared with that of SiGe. Typically, since the doping of the lightly doped emitter is 1-2 orders of magnitude above that of the collector, barriers at the collector edge become significant before barriers at the emitter edge, leading to the band structure of Figure 4.15. Applying an increased reverse bias to the collector-base junction depletes some of the boron which has outdiffused into the Si collector, leading to a smaller barrier [48].

A smaller barrier leads to increased collector current because more electrons diffusing across the base can climb over the smaller barrier. A device's Early voltage is directly related to increasing collector currents with increased base-collector bias. Thus, an outdiffused transistor will have a far lower Early voltage than a transistor without outdiffusion with identical base doping because its collector current is a strong function of base-collector reverse bias. Consequently, even an HBT with a base doped 10^{20} cm^{-3} can have a poor Early voltage due to the base-collector voltage modulating the height of the conduction band barrier which controls the collector current.

Mathematically one can explain this physical understanding through the use of Equation 2.4. The effects of boron outdiffusion on SiGe HBT saturation currents and Early voltages were extensively modeled prior to this thesis [48, 49, 51]. The simplest model of a base following boron outdiffusion would be a base consisting of half p-type SiGe and half p-type Si with both halves having identical doping, N_A . The SiGe section would be at the base-emitter interface while the Si base would be at the base-collector interface. The width, $(W/2)$, of each material as well as the doping, N_A , would be held

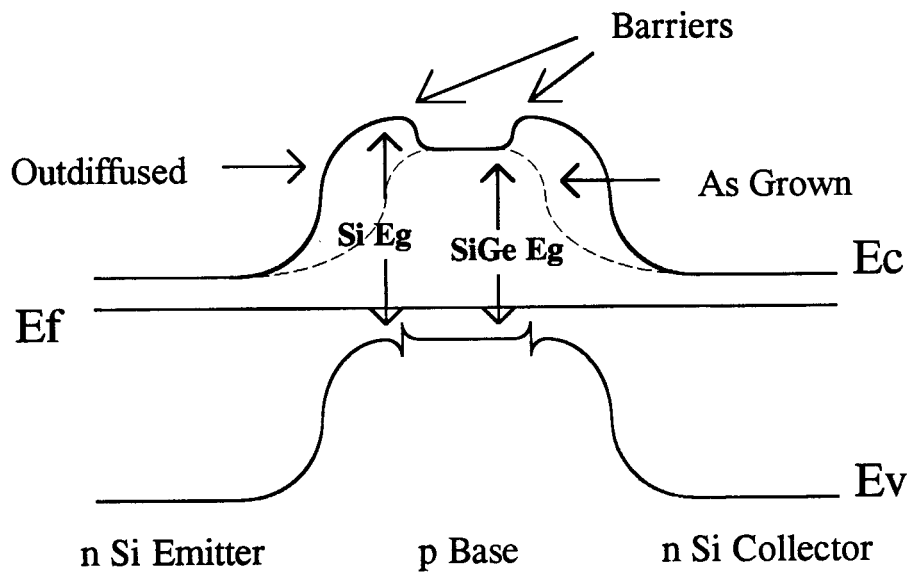


Figure 4.14: Band structure of an outdiffused SiGe HBT compared with that of a not-outdiffused HBT.

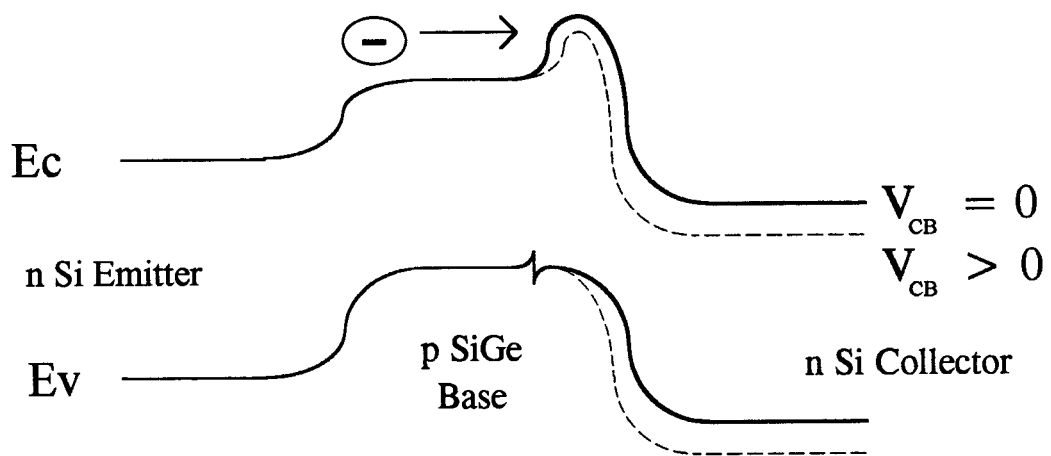


Figure 4.15: Outdiffused transistor showing a barrier at the base-collector interface being modulated by a base collector reverse bias.

fixed. The diffusion coefficients of electrons, D_n , would also be assumed constant in both materials. Under these assumptions, Equation 2.4 reduces to

$$J_C = \frac{2qD_n}{WN_A} \left(\frac{n_{i,Si}^2 n_{i,SiGe}^2}{n_{i,SiGe}^2 + n_{i,Si}^2} \right) e^{qV_{BE}/k_B T} \quad [4.2]$$

Taking the limit that $n_{i,SiGe}^2 \gg n_{i,Si}^2$, we are left with

$$J_C = \frac{2qD_n n_{i,Si}^2 e^{qV_{BE}/k_B T}}{WN_A} \quad [4.3]$$

So for this transistor, and outdiffused transistors in general, the collector current is dominated by the silicon part of the base and the fact that half of the base width is SiGe with the same doping level has no effect on the collector saturation current. In general, the base material with the largest bandgap determines the collector current in a bipolar transistor due to the exponential dependence of n_i^2 on bandgap (Equation 2.3). Hence outdiffused transistors will have lower collector saturation currents than transistors which have not outdiffused.

For an outdiffused transistor with a barrier height ϕ_0 and barrier width σ_0 at the base-collector edge L_0 , the collector current has been modeled as [48]

$$J_C = q \left(\frac{N_A}{n_i^2 D_n} dx + \frac{\sigma_0}{n_i D_n L_0} e^{q\phi_0/k_B T} \right)^{-1} e^{qV_{BE}/k_B T} \quad [4.4]$$

Hence, an outdiffused transistor will have a low V_A since increasing V_{BC} reverse bias leads to an increased J_C by reducing ϕ_0 and σ_0 .

4.4.2 Outdiffusion Experiments

To accommodate the inevitable diffusion of boron during both the emitter growth and other postgrowth processes, undoped SiGe spacer layers are incorporated surrounding the doped SiGe base so that the boron diffuses into SiGe rather than Si [47] (Figures 3.3 and 4.13). Figure 4.16a shows the electrical characteristics of devices grown using 50 Å spacers on either side of a 50 Å 10^{20} cm⁻³ boron doped Si_{0.8}Ge_{0.2} base. Applying a reverse bias of 1 V does not lead to any increase in collector current in the Gummel plot, a fact which is reflected by the high Early voltages of the common emitter characteristics. The high Early voltages are due to the high base doping which prevents the base-collector depletion region from causing significant changes in base width.

Figure 4.16b, on the other hand, shows electrical characteristics of an HBT which was grown identically to the previous one with the exception that it has 25 Å spacer widths. Applying a 1V reverse bias to the base collector increases the collector current by a factor of 2 and consequently the transistor's Early voltage has been degraded to ~0.5 V from ~50 V. While the boron diffusion is identical in both samples due to the identical growth conditions, in the 25 Å spacer transistor the boron moved into silicon rather than into SiGe as in the case of the 50 Å spacer devices. This boron diffusion into the n-type silicon collector leads to dramatically degraded electrical characteristics. This device comparison highlights the importance of spacer thickness and of maintaining control of boron diffusion during SiGe HBT process integration.

From the previous discussion it is apparent that the electrical characteristics of transistors are a more sensitive probe of boron diffusion than only SIMS. While SIMS is not able to resolve boron diffusion lengths of the order of 25 Å, changes in the expected collector saturation current and Early voltage of a transistor are immediate signs of

Fig. 4.16a: $\text{Si}_{0.8}\text{Ge}_{0.2}$ 50 Å Spacers

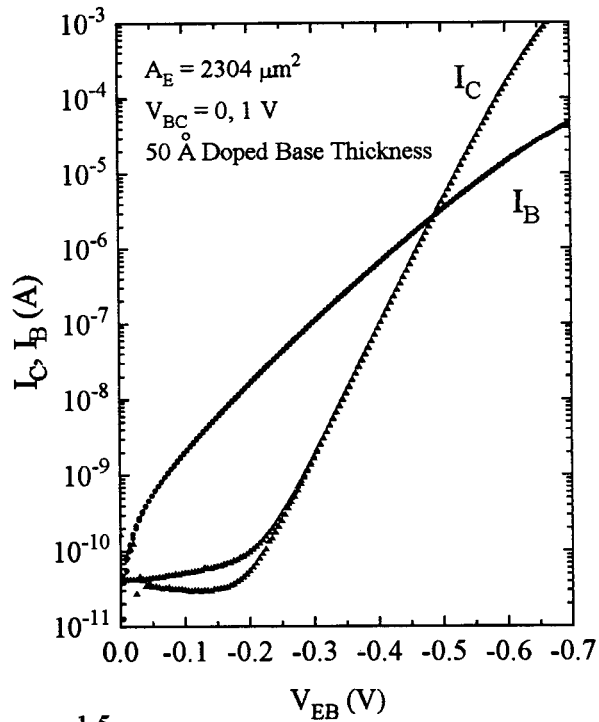


Fig. 4.16b: $\text{Si}_{0.8}\text{Ge}_{0.2}$ 25 Å Spacers

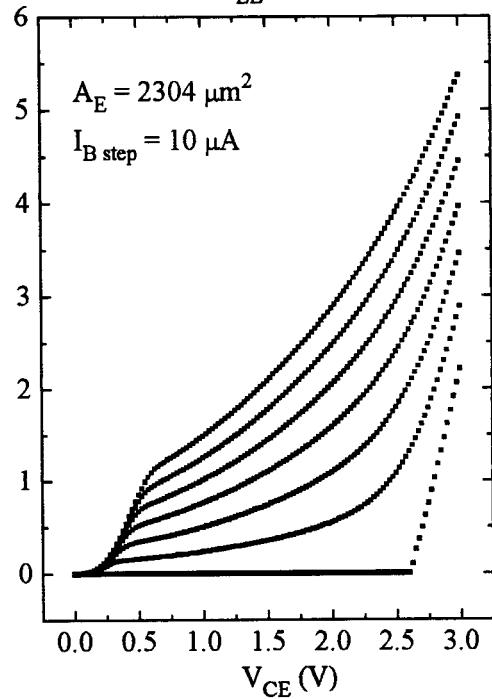
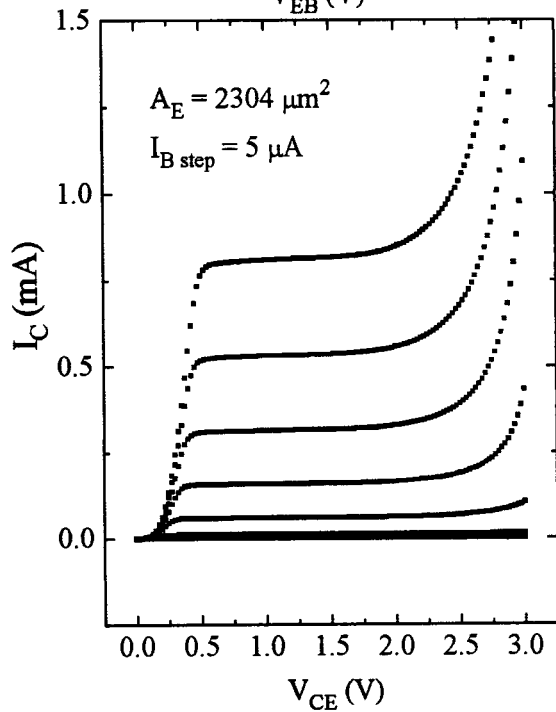
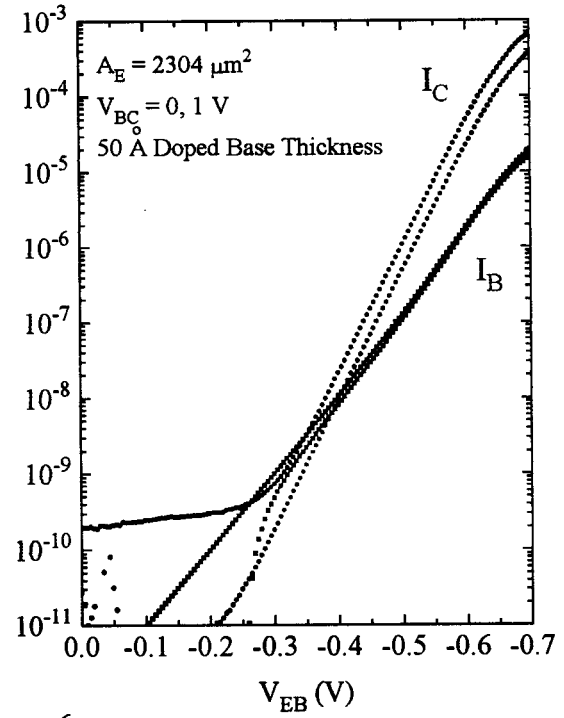


Figure 4.16: Transistor characteristics of HBTs with 50 and 25 Å spacers.

outdiffusion, even at 25 Å length scales. It is, however, important to exercise some caution in using these measurements. As one moves towards the edge of the 4 inch wafer, the wafer growth temperature is lower, leading to a decreased growth rate. Hence spacer thicknesses as well as doped base thicknesses decrease slowly towards the edge of the wafer.

Figure 4.17b shows characteristics of a transistor fabricated from pieces half way between the center and edge of a wafer with 50 Å spacers. Devices fabricated from material from the center of this wafer are known not to be outdiffused, as shown in Figure 4.17a. One can see a marked difference in the common emitter characteristics due to the onset of outdiffusion. Outdiffused common emitter curves similar to those of Figure 4.17b have been previously demonstrated [48]. Hence just because devices from the wafer center are not outdiffused does not necessarily imply that devices from the edge are not outdiffused because of the thinner spacer layers near the edge. The researcher using this reactor's epi material needs to be aware of the fact that wafers grown in this reactor can have varying device characteristics due to thickness nonuniformities.

To get an idea of the spacer thickness required to prevent outdiffusion, as well as of the nonuniformity inherent in Princeton's RTCVD growth chamber, Figure 3.5 plots growth rate as measured by TEM vs. distance from the center of a wafer for two different growth conditions. Note that a growth wafer has a radius of 5 cm. Hence any device fabricated from material halfway between the center and the edge of the wafer will have $\text{Si}_{0.8}\text{Ge}_{0.2}$ thicknesses ~35% and Si thicknesses ~20% less than that of devices fabricated from material at the center.

Hence the device from Figure 4.17b has ~ 35 Å spacer thicknesses, in contrast with the wafer from Figure 4.17a, which has spacer thicknesses of ~50 Å, even though both devices came from the same wafer.

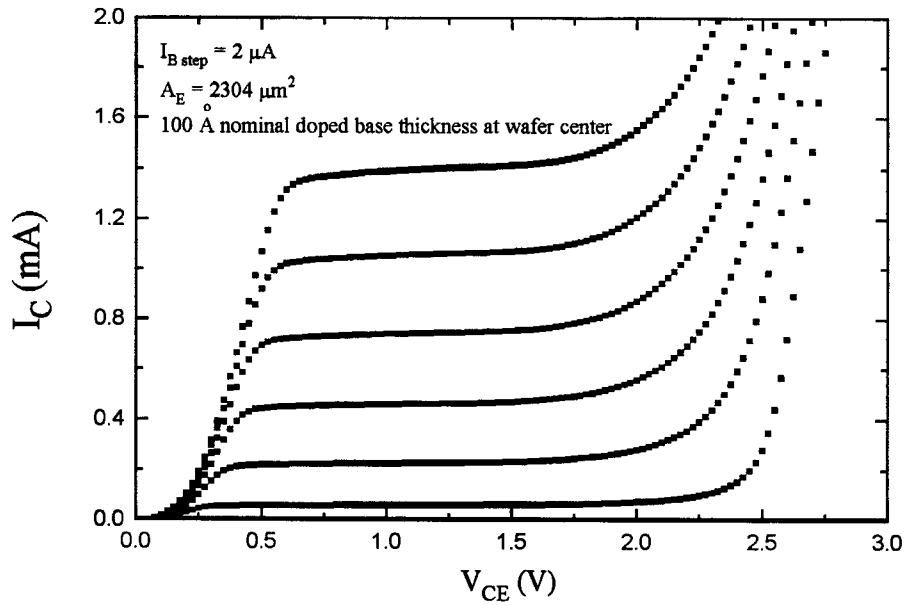


Figure 4.17a: Device from wafer center

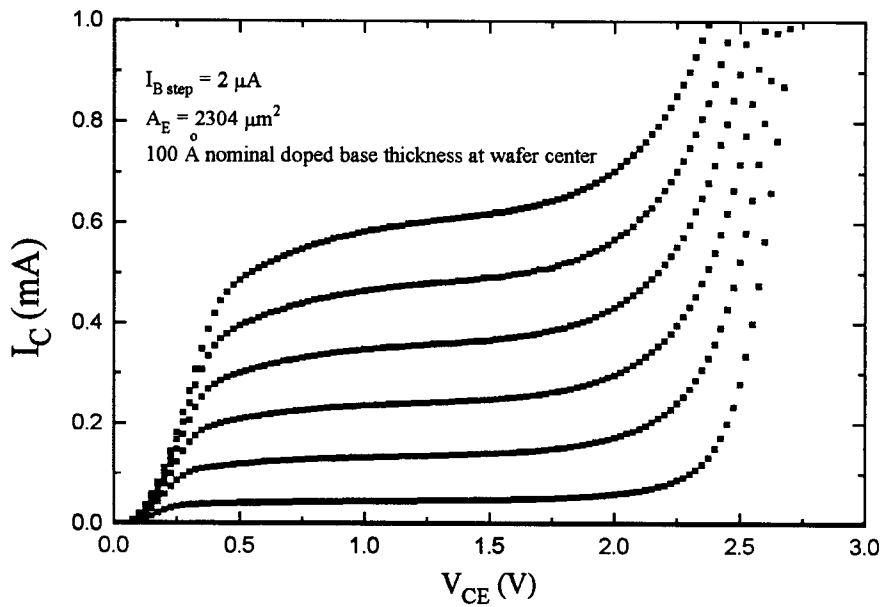


Figure 4.17b: Device from piece half way between wafer center and edge

Figure 4.17: Common-emitter characteristics from the center and halfway to the edge of the same $\text{Si}_{0.8}\text{Ge}_{0.2}$ HBT wafer.

One may conclude from this data and the data presented in Figure 4.16 that, in order to correctly predict the effects of outdiffusion on the transistor characteristics of $\text{Si}_{0.8}\text{Ge}_{0.2}$ devices, one needs to understand, and model correctly, the consequences of boron outdiffusion on device performance down to a level of tens of angstroms.

4.5 A Final Note

The common-emitter characteristics of the transistors used in this thesis display large ($\sim 0.5\text{V}$) V_{CE} offset voltages. This is due to the large collector series resistance due to the low subcollector n-type doping and the high collector contact resistance. These resistances seriously limit the amount of forward base-collector current at fixed base-collector forward bias required to drive the transistor into saturation.[52] Large V_{CE} offset voltages of $\sim 0.5\text{ V}$ have also existed in previous double-mesa Princeton HBTs fabricated using lightly doped subcollectors, however. [15]

Before concluding this section it is necessary to note that undoped spacer layers surrounding SiGe is yet another tradeoff in device performance vs. materials science. While these spacers are necessary to prevent outdiffusion, they consume total base critical thickness without contributing to a reduction of base sheet resistance because they are not doped. Hence one cannot use arbitrarily large spacer thicknesses due to critical thickness limitations. Enhancing SiGe critical thickness would be desirable to relax these tradeoffs. This topic will be addressed in Chapters 5 and 6. Reducing boron diffusion will be discussed in Chapter 7.

4.6 Summary

This chapter has served to introduce the real world problems a SiGe HBT researcher faces due to process and equipment constraints. The subject of non-ideal base currents was focused on using an investigation of three different emitter structures. SiGe HBTs with heavily-doped single-crystalline phosphorus emitters containing a background oxygen concentration of $\sim 10^{20} \text{ cm}^{-3}$ were shown to have quasi-ideal base current characteristics despite an unpassivated double-mesa structure.

The degradation in SiGe HBT electrical characteristics due to boron outdiffusion was established. The chapter finished with a discussion of the experimental limitations caused by SiGe thickness non-uniformities due to wafer temperature variations.

Introduction to Carbon in Si and Si_{1-x}Ge_x

5.1 Motivation for Carbon in Si-based Alloys

The finite critical thickness of SiGe causes transistor design tradeoffs between base thickness, spacer thickness, Ge fraction, and base doping concentration. Loosening this critical thickness limitation would be a desirable step forward for SiGe HBTs as well as for other devices built from SiGe. The fact that germanium is a larger atom than Si gives rise to the strain in SiGe which limits critical thickness. A substitutional carbon atom, however, is both isoelectronic and smaller than both Si and Ge. Diamond has a lattice parameter of 3.546 Å compared to 5.43 Å for silicon or 5.66 Å for germanium. Hence incorporating substitutional carbon atoms into Si_{1-x}Ge_x alloys, forming the new alloy Si_{1-x-y}Ge_xC_y, would be expected to reduce the strain in Si_{1-x}Ge_x. Previous workers have shown that 1% C in Si compensates the strain of 8.3-10% Ge [53, 54]. Hence a typical 20% Ge HBT would be lattice matched to a Si wafer if it contains approximately 2% C. This material would be desirable from a device point of view since the critical thickness constraint limiting spacer thickness and base width would now be lifted.

5.2 Early Work on Carbon in Silicon

However, from previous research on C in Si, one would not expect encouraging results from C in SiGe. The fundamental problem associated with carbon in Si is that while Ge is completely miscible in Si, the solid solubility of C in Si is $4 \times 10^{17} \text{ cm}^{-3}$ at the melting point of silicon [55]. SiC, the stable form of C in Si, will tend to form at concentration levels higher than this. As a result of the low solubility of C in Si, workers prior to the early 1990's regarded carbon as a contaminant.

Reviews of older work on carbon center on carbon in as-grown silicon wafers [56] and focus on measuring the diffusion coefficient of carbon in silicon and the effects of high temperature heat treatments on carbon in silicon. Gosele reviewed work on the interaction of point defects with carbon [57]. Early work on C in Si centered on the measurement of the effect of carbon on the silicon lattice constant [58], of the solubility of carbon in silicon [59] and of the diffusivity of carbon in silicon [60]. It was shown that 10^{18} cm^{-3} carbon atoms in silicon wafers form SiC precipitates following a 900°C , 160 minute anneal [61]. Research on the effects of carbon on electrical device properties showed that 10^{17} cm^{-3} carbon atoms in as-grown wafers caused degradation of diode breakdown voltages due to SiC precipitation following 1300°C anneal for 119 hours [62]. A review of the effect of $5 \times 10^{16} \text{ cm}^{-3}$ carbon concentrations on electrical devices focused on the degradation in device performance caused by high temperature (1200°C , 15 hours) processed induced "swirl" defects [63].

5.3 RTCVD Growth of $\text{Si}_{1-x-y}\text{Ge}_x\text{C}_y$ Alloys at Princeton

If, however, some method could be used to incorporate carbon on substitutional silicon lattice sites without forming SiC or carbon precipitates, carbon could possibly find applications in silicon technology. The SiGeC thin films studied in this thesis are fundamentally different from those produced in prior work because the C is now incorporated in SiGe epitaxially and grown at a low temperature with the hope that more carbon atoms will become substitutional. The SiGeC alloy layers used in this study were grown at 625°C using the identical growth process as that for the SiGe control devices except that the methylsilane flow was adjusted to provide a variable carbon fraction in both the base spacer layers and the doped base. The highest thermal budget to which the as-grown SiGeC layers were exposed occurred during the ~ 70 minute 700°C emitter growth. Note that these thermal budgets are far lower than those typical of prior C in Si research. It is hoped that by metastable epitaxial growth and low temperature processing, the incorporation of large carbon concentrations may become possible without degrading the device electrical properties.

One can measure the amount of substitutional carbon in a SiGeC layer by measuring the shift in X-ray peak from the SiGe control wafer and assuming that 1% substitutional C compensates the strain of 8.3% Ge. This method also assumes that carbon incorporation has no effect on the germanium fraction of the ~ 400 Å layer. Figure 5.1 shows X-ray spectra from a $\text{Si}_{0.75}\text{Ge}_{0.25}$ control wafer as well as from several SiGeC wafers with varying carbon fractions. The X-ray shift between the SiGe peak and the Si substrate peak is used to determine the germanium fraction via the expression $x = 0.178 \times \Delta(2\theta)$ [16] for (400) diffraction peaks. As carbon is added to SiGe, the peaks shift towards the Si substrate peak indicating a reduction in lattice constant. Thus the amount

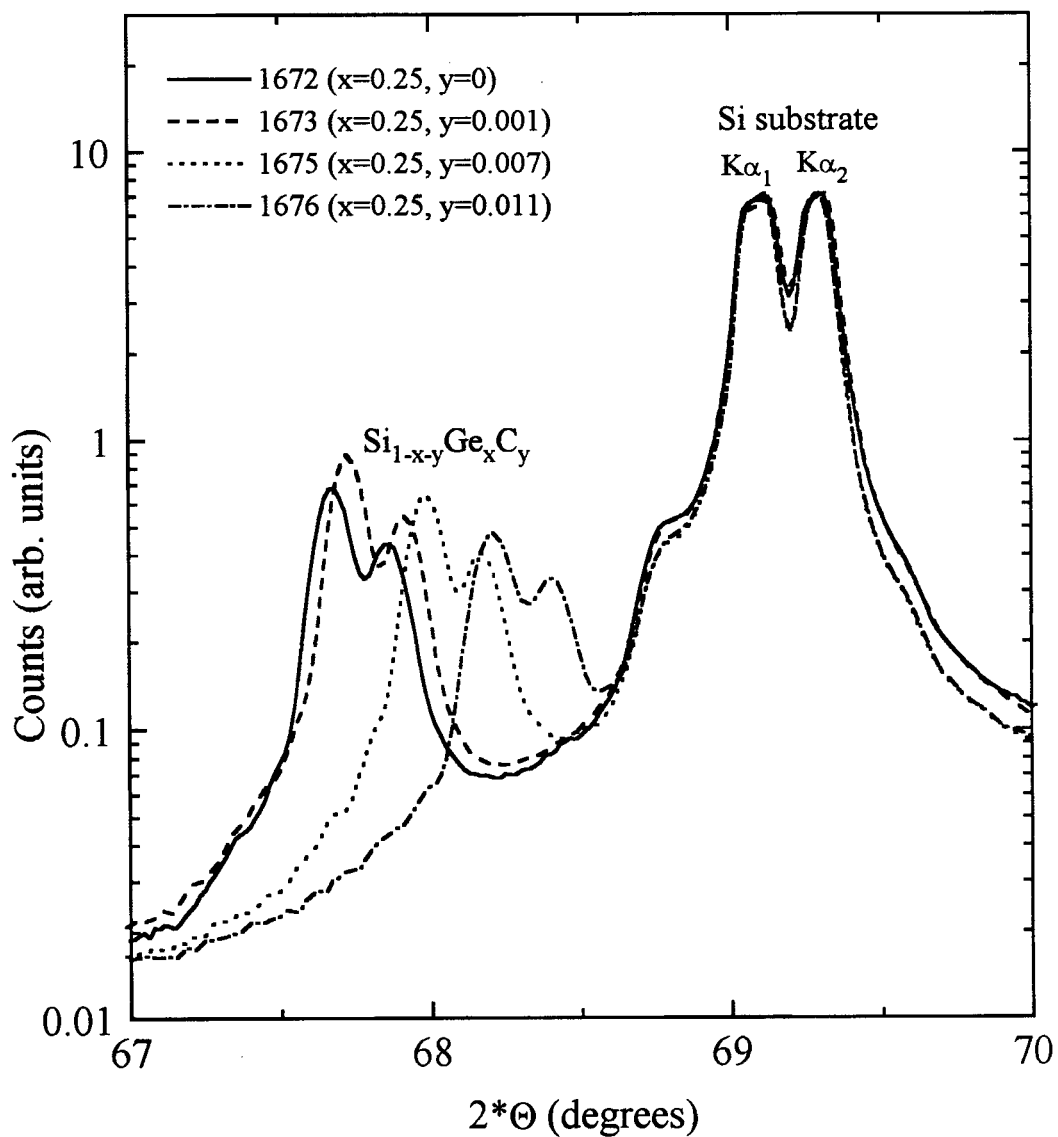


Figure 5.1: X-Ray diffraction spectra (400 peaks) of HBT wafers grown with varying carbon fractions.

of substitutional carbon can be extracted assuming identical germanium fractions in all of the wafers and that 1% C compensates the strain of 8.3% Ge.

The total incorporated carbon concentration may be measured by SIMS, as shown in Figure 5.2 for a 0.5% C sample (as measured by X-ray). The SIMS value for this sample is $\sim 2 \times 10^{20} \text{ cm}^{-3}$ or $\sim 0.4\%$. Note that SIMS shows that carbon, like boron and germanium, turns on and off abruptly [42]. SIMS and X-ray measurements of carbon fractions do not always agree as well as would be expected, however, and in this thesis the carbon levels given are those measured by X-ray. X-ray measurements have been chosen because the X-ray technique makes only the theoretical assumption that 1% C compensates the strain of 8.3% Ge, and SIMS requires an additional carbon calibration sample to extract the carbon fraction.

The difference between the carbon fraction as measured by SIMS and that measured by X-ray could be expected to give the interstitial carbon fraction. However, the question of interstitial vs. substitutional carbon is not the focus of this work and, in any case, unambiguous data on the subject of interstitial carbon have yet to be published.

Boron incorporation in UHVCVD epitaxy using diborane and silane is known to be a linear function of flow rate from 10^{18} cm^{-3} to $5 \times 10^{20} \text{ cm}^{-3}$ at a growth temperature of 550°C [42, 64]. Substitutional carbon incorporation vs. flow rate is also linear in flow rate for carbon fractions below 1%, as shown in Figure 5.3 which plots carbon incorporation vs. methylsilane flow for the samples used in this thesis. Reports have been published [55, 20] which contend that beyond 1% carbon fraction, the correlation between substitutional carbon (as measured by X-ray) and methylsilane flow is nonlinear. That is doubling the methylsilane flow does not double the substitutional carbon content. Bodnar et. al. believe that the total incorporated carbon fraction (as measured by X-ray) is actually a linear function of methylsilane flow and that the difference between the total

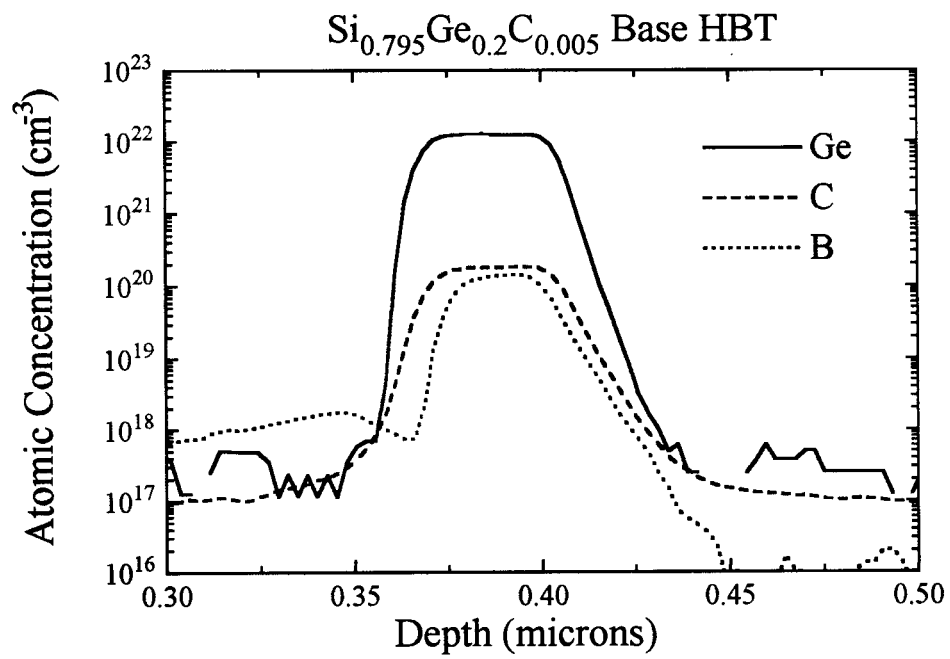
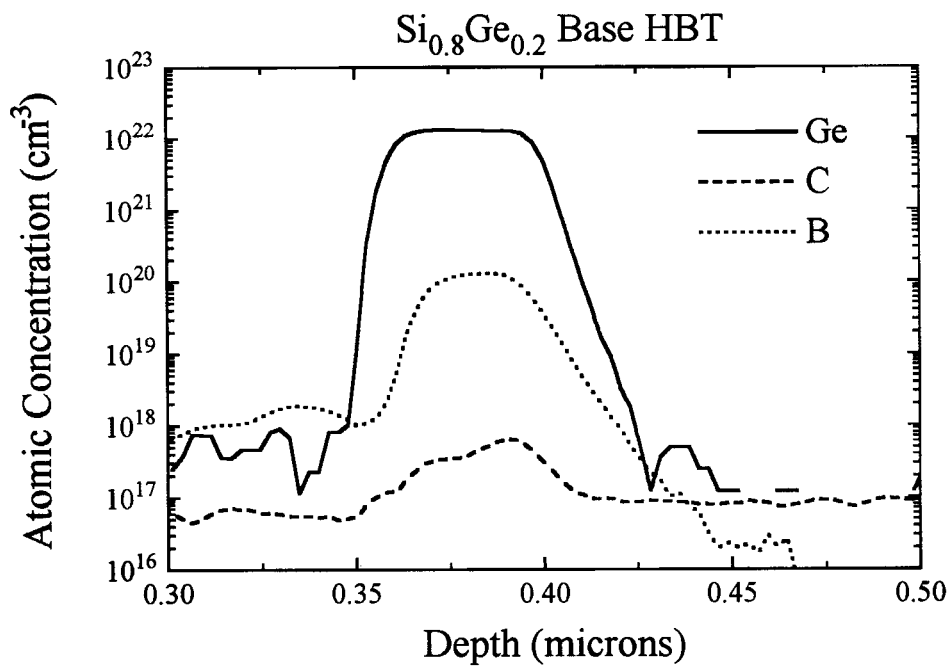


Figure 5.2: SIMS of SiGe and SiGeC bases.

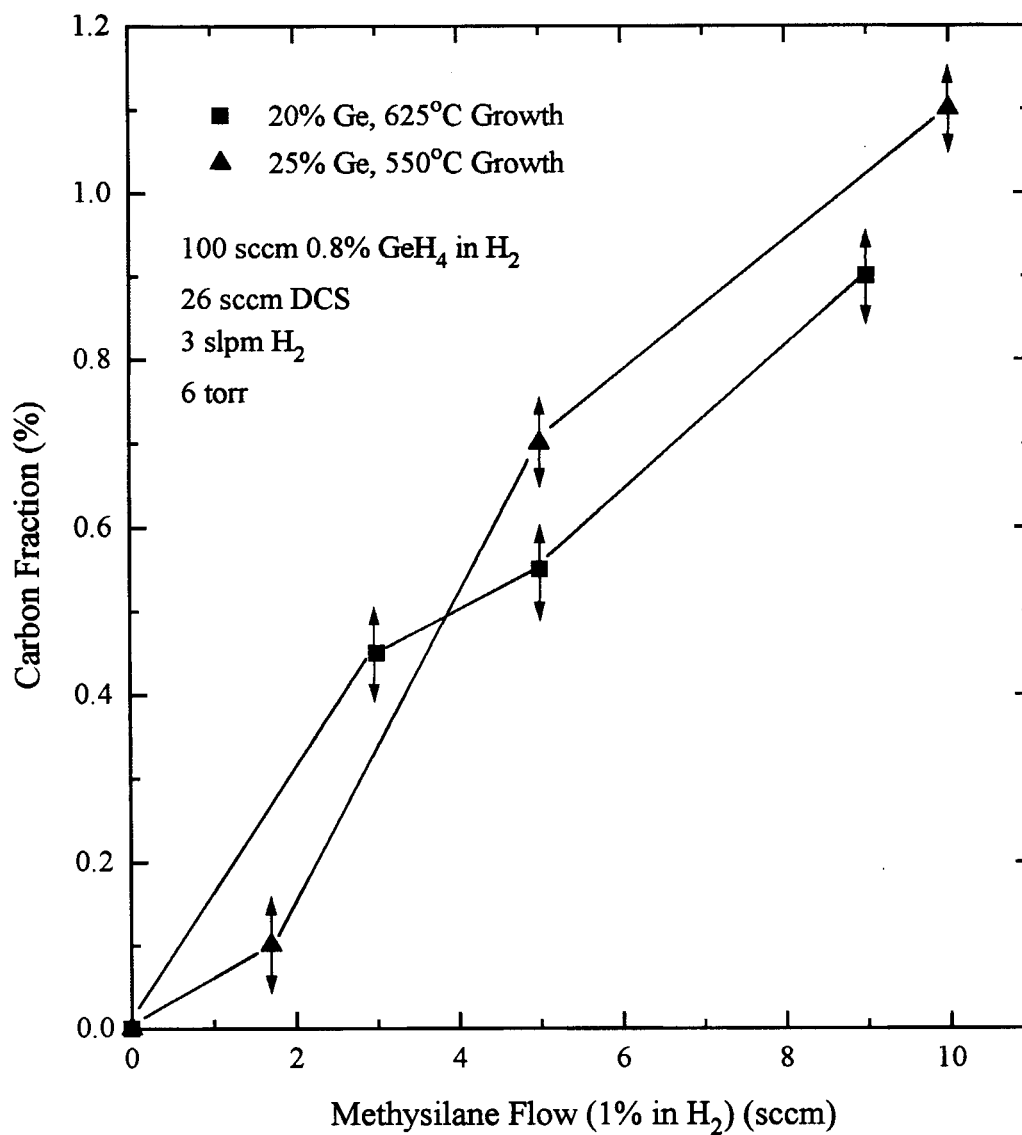


Figure 5.3: Substitutional carbon fraction as measured by XRD vs methylsilane flow for the HBTs used in this thesis.

incorporated carbon fraction and the substitutional carbon fraction is incorporated as interstitial carbon [55].

Figure 5.4 shows the X-ray diffraction from a 1.9% C sample with 25% Ge, grown by C.W. Liu, which is the sample with the highest convincingly measured carbon fraction grown at Princeton. Cross section TEM micrographs of this sample taken at University of Virginia by Eric Stach show the layers to be defect-free even at this large carbon fraction, as shown in Figure 5.5.

5.4 Review of Research on Si-based Carbon Alloys

The alloy $\text{Si}_{1-x}\text{C}_x$ was first grown in 1992 at IBM by molecular beam epitaxy at low temperatures of 500-600°C and low carbon fractions of 0.5% [65]. These films were used to demonstrate that SiC precipitates form at annealing temperatures above 1000°C [66]. The growth of $\text{Si}_{1-x}\text{C}_x$ alloys with up to 3 % carbon levels has also been demonstrated [67, 68]. $\text{Ge}_{1-x}\text{C}_x$ alloys have also been demonstrated on silicon substrates by UHVCVD with $C < 5\%$ [69] and by MBE with $C < 3\%$ [70].

However, the bulk of recent carbon work has focused on the alloy SiGeC grown by CVD methods with carbon fractions below 2%. Broad interest in SiGeC low temperature epitaxy by CVD started about 1994 following the publication of CVD SiGeC epilayers with ~ 0.6 % C grown using methylsilane as the carbon source [53]. There have been three intensive review papers on SiGeC published thus far [55, 71, 72]. While the alloy SiGeC was first demonstrated by MBE in 1992 [54], Princeton's interest in SiGeC began following the first demonstration of SiGeC grown by CVD using methylsilane as the carbon source [53]. In 1994 the first SiGeC layers under tensile stress, that is the lattice

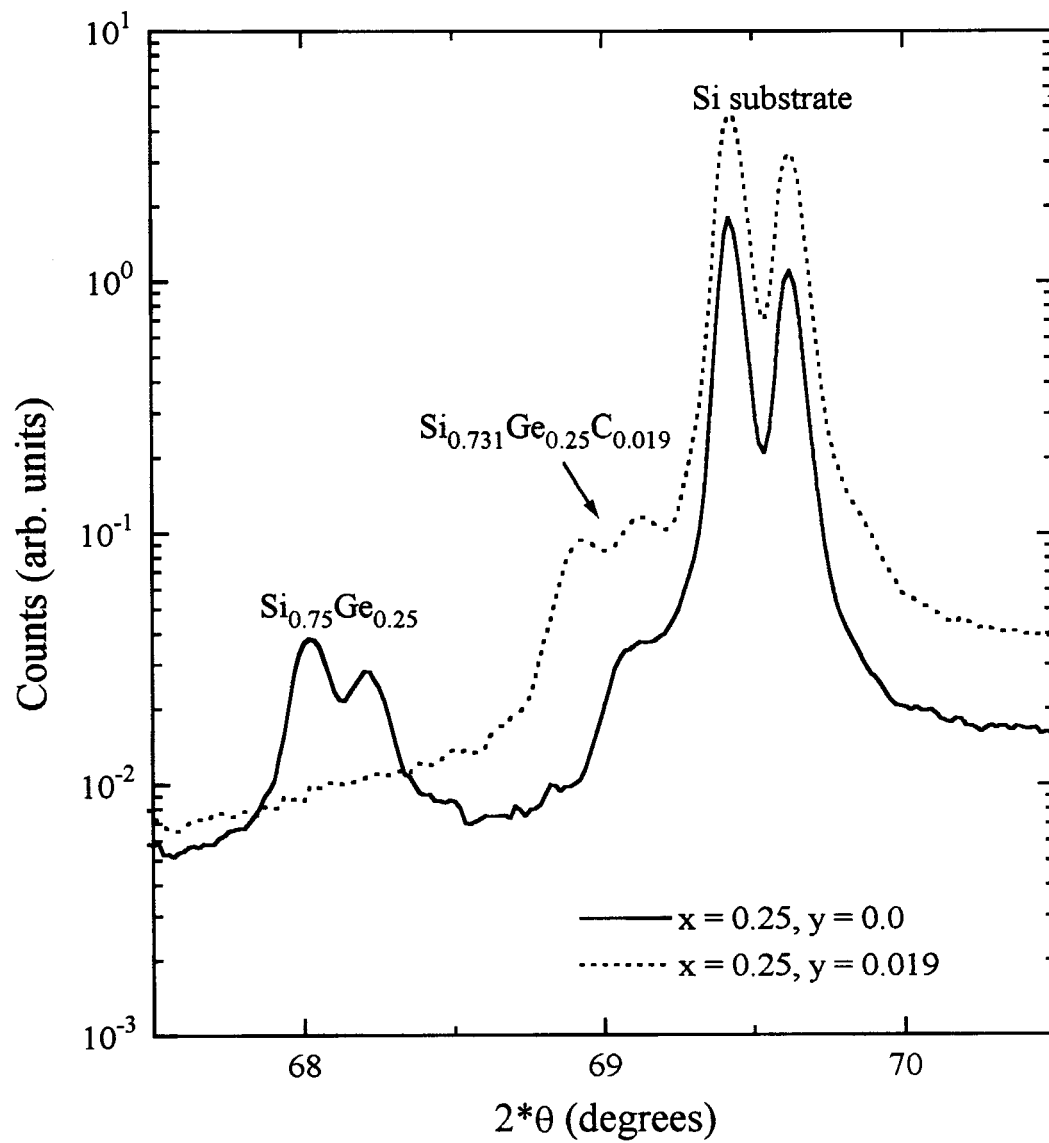


Figure 5.4: X-Ray diffraction spectra of 1.9% carbon sample.

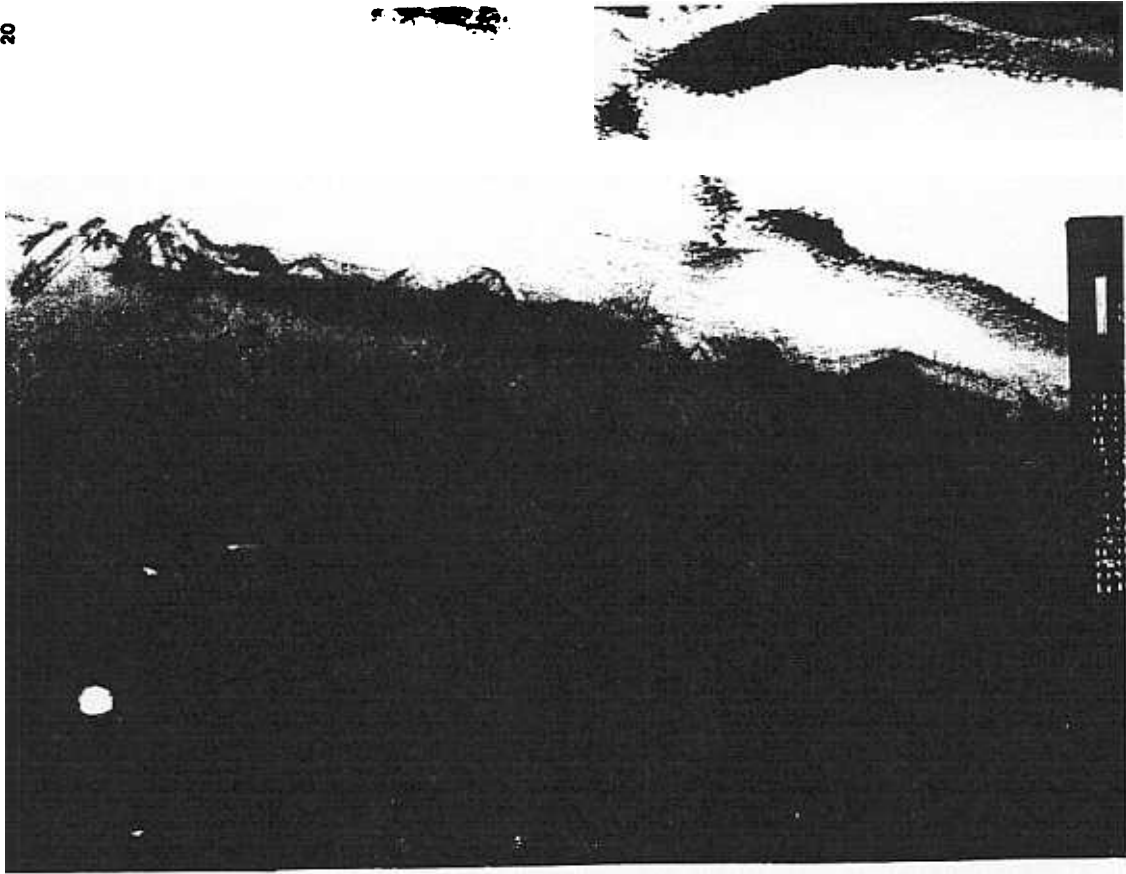


Figure 5.5: Cross section TEM micrograph of Si 0.731 Ge 0.25 C 0.019 epilayers.

spacing in the growth direction is smaller than that of Si, were demonstrated by MBE [73].

While Princeton's research has, until now, focused on the carbon precursor methylsilane, extensive research has been conducted using novel precursors such as tetrasilane, $(\text{C}(\text{SiH}_3)_4)$ [74], and methyl germane, $(\text{GeH}_3\text{CH}_3)$ [75]. SiGeC layers have also been fabricated by solid phase epitaxy using carbon implants into strained SiGe alloys and subsequent annealing [76, 77]. In addition to $\text{Si}_{1-x}\text{C}_x$, $\text{Ge}_{1-x}\text{C}_x$, and $\text{Si}_{1-x-y}\text{Ge}_x\text{C}_y$, work has also begun on alloys containing tin to form $\text{Si}_{1-x-y}\text{Sn}_x\text{C}_y$ [78].

A review of silicon based optoelectronics and optical properties of silicon alloys has been published by Soref [79]. The bandgap of SiGeC was first measured optically using the first bandedge luminescence of SiGeC in 1994 [80]. This was followed by Princeton work showing defect-free SiGeC photoluminescence for carbon fractions less than 1.1% published by St. Amour in 1995 [81]. Photoluminescence from $\text{Si}_{1-x-y}\text{Ge}_x\text{C}_y/\text{Si}_{1-x}\text{C}_x$ quantum well layers have been demonstrated as well [82], along with intersubband absorption in $\text{Si}/\text{Si}_{1-x-y}\text{Ge}_x\text{C}_y$ quantum wells with C levels of $\sim 1\%$ [83]. Considering other Si-based alloys, bandedge photoluminescence from $\text{Si}_{0.96}\text{Sn}_{0.04}$ has been measured [84] and the optical properties of $\text{Ge}_{1-x}\text{C}_x$ alloys have also been investigated [85, 86]

The first SiGeC electrical devices were demonstrated by Princeton in 1994 using SiGeC alloy base HBTs [87]. Since then a variety of devices using SiGeC have been investigated ranging from MOS capacitors [88], photodetectors [89], and Schottky diodes [90]. $\text{Si}_{1-x}\text{C}_x$ has been used in p-n junctions [91] as well as in quantum wells to demonstrate modulation doping [92].

5.5 Strain Compensation by Boron

One should recognize that strain compensation of SiGe is not limited to carbon. Researchers have also used boron atoms to form the alloy $\text{Si}_{1-x-y}\text{Ge}_x\text{B}_y$ [93, 94]. It has been shown that 1% boron compensates the strain of 6% germanium [95]. While $\text{Si}_{1-x-y}\text{Ge}_x\text{B}_y$ films grown with 5.8% germanium have extended defects [95], other workers have grown Si/Si_{1-x}B_x alloy superlattices with $5 \times 10^{21} \text{ cm}^{-3}$ *electrically active* boron concentrations by UHVCVD which are defect-free [42]. These boron fractions form precipitates following an 800°C anneal, however.

5.6 Summary

Carbon in silicon has been introduced. Early work on carbon in silicon was reviewed to provide a background of why carbon in SiGe may be problematic. The Princeton approach to $\text{Si}_{1-x-y}\text{Ge}_x\text{C}_y$ epitaxy is established. A review of current work in $\text{Si}_{1-x-y}\text{Ge}_x\text{C}_y$ is presented to give a perspective of where the alloy may find potential applications.

Measurement of $\text{Si}_{1-x-y}\text{Ge}_x\text{C}_y$ Bandgap Using HBTs

6.1 Introduction

Theoretically, while a $\text{Si}_{0.78}\text{Ge}_{0.2}\text{C}_{0.02}$ -base HBT will be lattice matched to the silicon substrate, the bandgap of this new material must be measured in order to predict the device electrical characteristics. The approach used in this thesis work was to fabricate the first SiGeC HBTs and use changes in the device electrical characteristics to measure the effect of carbon on the bandgap of SiGe. From Equations 2.2 and 2.3 one can see that changes in bandgap may be extracted from changes in a device collector saturation current due to the dependence of n_i on bandgap.

Figure 2.3 shows the bandgap of strained SiGe vs. Ge content. Any mechanism used to relax the strain in this layer, such as carbon incorporation or dislocation formation, will shift the bandgap up, at fixed Ge fraction, towards that of unstrained SiGe. Hence if one adds carbon to reduce the strain and thus increase critical thickness in a SiGe layer, one should also expect to lose some bandgap offset due to the change in strain of the

layer. One might also expect that the substitutional carbon atom itself would also affect the bandgap. Hence, the change in bandgap between SiGeC and SiGe will be due to both the effect of strain relaxation and the effect of the carbon atom.

6.2 Transistor Characteristics of $\text{Si}_{1-x-y}\text{Ge}_x\text{C}_y$ HBTs

Figure 6.1 shows common emitter characteristics of a $\text{Si}_{0.795}\text{Ge}_{0.2}\text{C}_{0.005}$ device as well as a $\text{Si}_{0.8}\text{Ge}_{0.2}$ control device. The high Early voltages imply no boron outdiffusion in these wafers, so that the collector saturation current at $V_{\text{BC}} = 0$ will not include the effects of barriers at the base-collector junction. Note, however, that the gain of the SiGeC device is roughly one half that of the SiGe device. From the common emitter characteristics of the transistors, one cannot determine at fixed V_{BE} whether this decrease in gain is due to an increase in base current, a decrease in collector current, or due to both.

Figure 6.2 shows the common-base characteristics of SiGeC devices with carbon fractions of 0.045%, 0.055%, and 0.09%. Note that the collector saturation current drops with increasing carbon fraction indicating a possible increase in base bandgap with increasing carbon levels. At roughly 0.5% C, the collector saturation current has decreased by a factor of 1.25 while at 0.9% C the collector current has decreased by a factor of 2.

Note that while the base current is non-ideal due to the oxygen at the base-emitter interface, the base currents at high V_{BE} increase monotonically with carbon fraction. At $V_{\text{BE}} = 0.7 \text{ V}$, $I_{\text{B}}(0.45\% \text{C}) = 2.8$, $I_{\text{B}}(0.55\% \text{C}) = 4.6$, and $I_{\text{B}}(0.9\% \text{C}) = 10.6$ times that of the no carbon sample. Hence while the DC gain of a SiGeC device with 0.9% C has

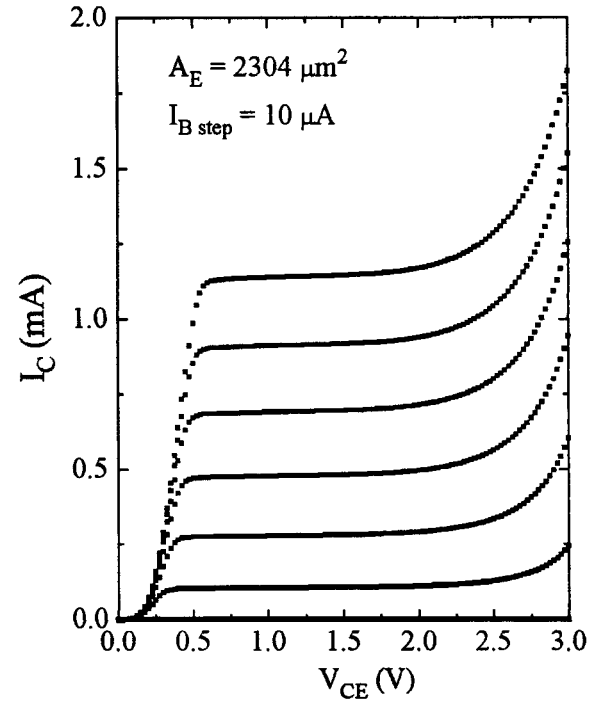
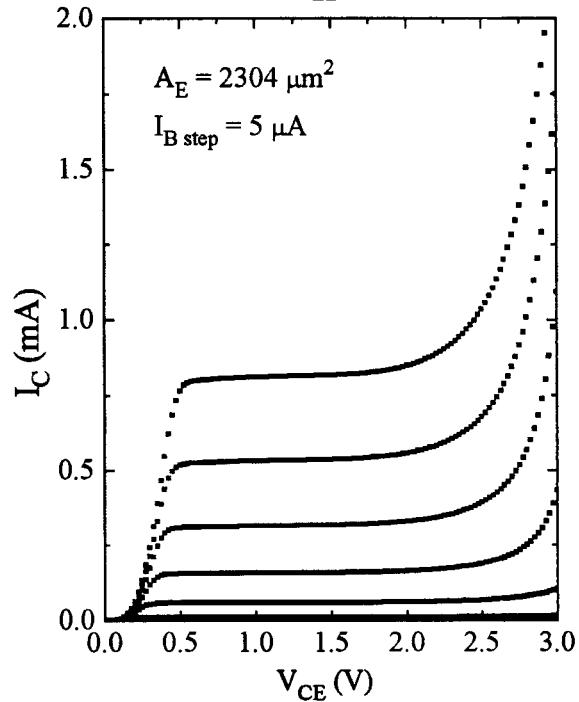
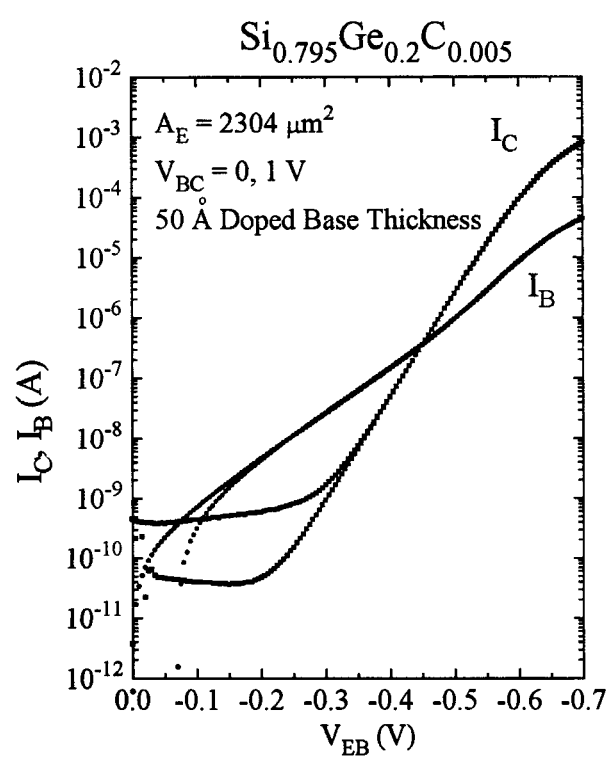
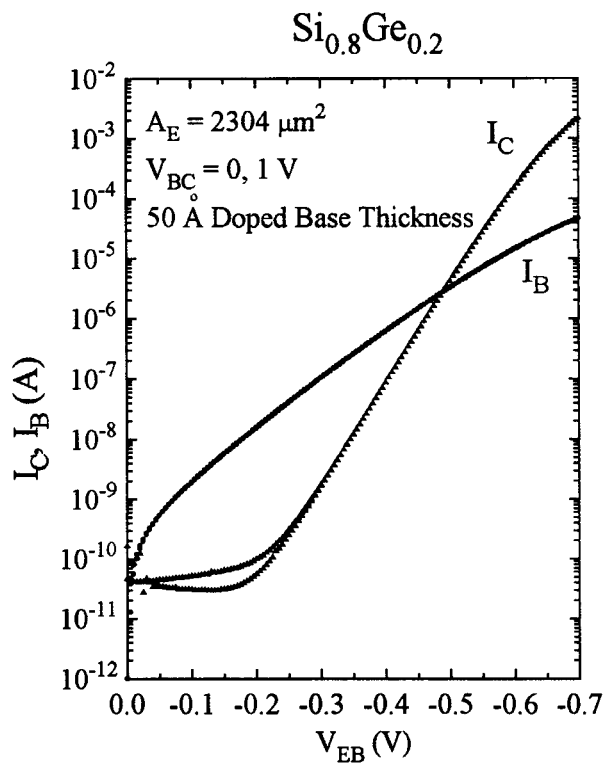


Figure 6.1: Electrical characteristics of $\text{Si}_{0.8}\text{Ge}_{0.2}$ and $\text{Si}_{0.795}\text{Ge}_{0.2}\text{C}_{0.005}$ devices.

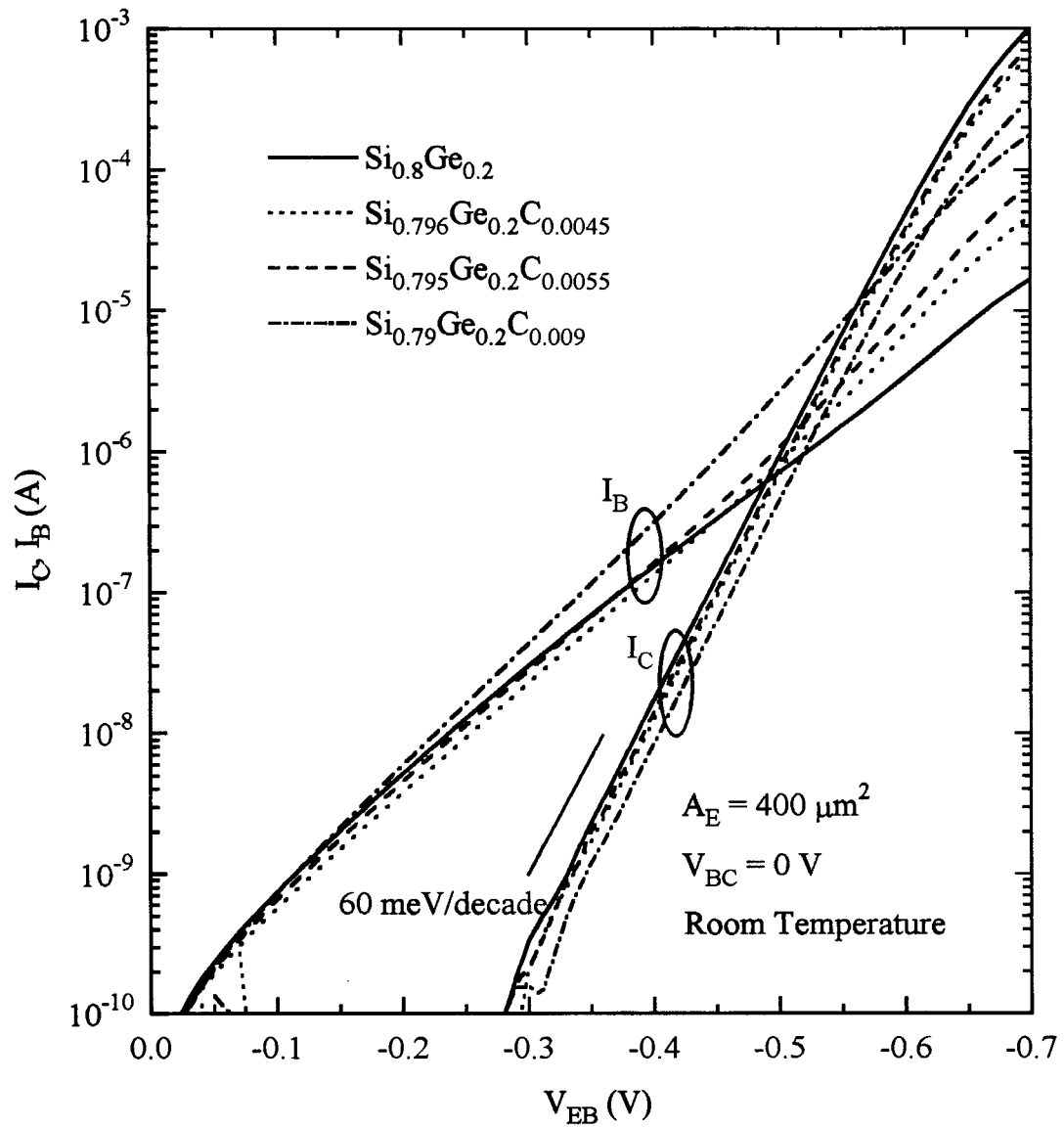


Figure 6.2: Common base characteristics for transistors with different carbon fractions.

declined by a factor of ~30, the largest decrease in current gain is caused by an increase in base current rather than a decrease in collector current.

6.3 Effect of Carbon on Si_{1-x}Ge_x Bandgap

The decreasing collector saturation currents with increasing C fraction may be a sign of increasing base bandgap with increasing carbon, as seen from Equation 2.2. However, changes in N_C , N_V , D_n , and N_A due to carbon incorporation may also cause changes in collector saturation current. By measuring the temperature dependence of the collector saturation currents of both SiGeC and SiGe devices, one can eliminate the effect of changes in N_C , N_V , D_n and N_A to extract ΔE_G , the change in bandgap between SiGeC and SiGe. Ratioing the collector current of SiGeC to SiGe at fixed V_{BE} gives

$$\frac{J_{C,SiGeC}}{J_{C,SiGe}} = \frac{D_{n,SiGeC} n_{i,SiGeC}^2 N_{A,SiGe} W_{B,SiGe}}{D_{n,SiGe} n_{i,SiGe}^2 N_{A,SiGeC} W_{B,SiGeC}} \quad [6.1]$$

Since,

$$n_{i,base}^2 = N_{C,base} N_{V,base} e^{-E_{G,base}/k_B T} \quad [6.2]$$

$$\frac{J_{C,SiGeC}}{J_{C,SiGe}} = k e^{\Delta E_G/k_B T} \quad [6.3]$$

Hence if we assume that the temperature dependence of N_C and N_V and D_n are identical in both SiGe and SiGeC, the prefactor reduces to a constant as the temperature of the

device is changed. The assumption that the prefactor k is independent of temperature is relatively reasonable and has been applied to accurately measure the bandgap difference between Si and SiGe using SiGe HBTs in the past [11, 96, 97]. Since the bandgap of SiGeC and SiGe is also temperature dependent [98], this technique also assumes that the bandgap difference between SiGeC and SiGe is a constant, independent of temperature. Although the bandgap difference between unstrained SiGe and Si is known to be constant, independent of temperature [11], the bandgap difference between strained SiGeC and strained SiGe has not been independently measured as a function of temperature. Since the prefactor k in Equation 4.3 is assumed to be independent of temperature, the slope of $\log(I_{C,SiGeC}/I_{C,SiGe})$ vs. $1/T$ is proportional to ΔE_G .

Figure 6.3 shows the collector currents of a $\text{Si}_{0.743}\text{Ge}_{0.25}\text{C}_{0.007}$ -base HBT as a function of temperature. Note that the slope of collector current is a measure of the temperature of the device, assuming an ideal collector current (Equation 2.1), and that the slope of the collector current increases with decreasing temperature. The decreasing collector saturation currents reflect changes in Equation 2.2 with temperature.

Figure 6.4 shows $\log(I_{C,SiGeC}/I_{C,SiGe})$ vs. inverse temperature. The negative slope of the data indicates that as carbon is added to SiGe, the bandgap increases, as one would expect from the changes in collector current at fixed temperature (Figure 6.2). The negative slope increases with increasing carbon fraction, indicating that the bandgap continues to increase as carbon fraction increases. One may extract ΔE_G for each carbon fraction from the slope. Figure 6.5 plots this bandgap difference for a variety of different carbon and germanium levels. A best fit line gives a slope of $\Delta E_G = +26 \text{ meV}/\%C$. This result corresponds quite well with previous photoluminescence data which measured a ΔE_G of $+21 \text{ meV}/\%C$ [81]. Since the $\text{Si}_{1-x-y}\text{Ge}_x\text{C}_y$ bandgap as measured by photoluminescence agrees with the HBT transport experiment, the bandgap must be

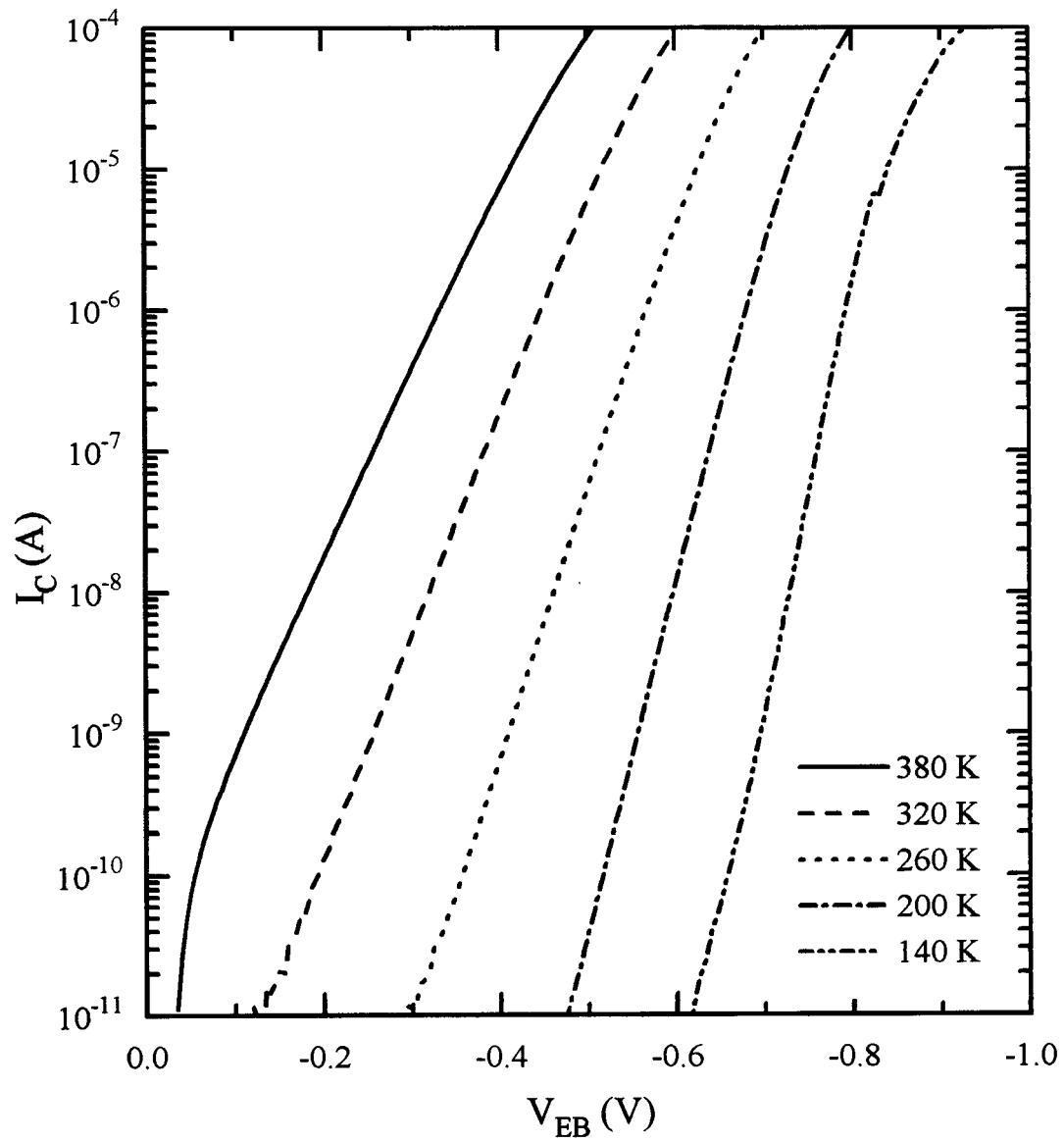


Figure 6.3: $\text{Si}_{0.743}\text{Ge}_{0.25}\text{C}_{0.007}$ collector currents as a function of temperature.